Published in final edited form as:

Neuron. 2021 November 17; 109(22): 3619–3632.e5. doi:10.1016/j.neuron.2021.08.015.

Experience-dependent myelination following stress is mediated by the neuropeptide dynorphin

Lindsay A. Osso[1,2], **Kelsey A. Rankin**[1], **Jonah R. Chan**[1,2,*]

[1]Weill Institute for Neurosciences, Department of Neurology, University of California, San Francisco, San Francisco, CA 94143, USA.

[2]Neuroscience Graduate Program, University of California, San Francisco, San Francisco, CA 94158, USA.

SUMMARY

Emerging evidence implicates experience-dependent myelination in learning and memory. However, the specific signals underlying this process remain unresolved. We demonstrate that the neuropeptide dynorphin, which is released from neurons upon high levels of activity, promotes experience-dependent myelination. Following forced swim stress, an experience that induces striatal dynorphin release, we observe increased striatal oligodendrocyte precursor cell (OPC) differentiation and myelination, which is abolished by deleting dynorphin or blocking its endogenous receptor, kappa opioid receptor (KOR). We find dynorphin also promotes developmental OPC differentiation and myelination, and demonstrate that this effect requires KOR expression specifically in OPCs. We characterize dynorphin-expressing neurons and use genetic sparse-labeling to trace their axonal projections. Surprisingly, we find they are unmyelinated normally and following forced swim stress. We propose a new model whereby experience-dependent and developmental myelination is mediated by unmyelinated, neuropeptide-expressing neurons that promote OPC differentiation for the myelination of neighboring axons.

ETOC BLURB

Recent studies have implicated experience-dependent myelination in learning and memory but the mechanisms regulating this process are unknown. Osso et al. identify the neuropeptide dynorphin as a novel regulator of experience-dependent myelination following stress.

*Lead Contact: jonah.chan@ucsf.edu.

AUTHOR CONTRIBUTIONS

L.A.O. and J.R.C. conceived of and designed all experiments. K.A.R. contributed to tissue processing, immunostaining, and imaging for Figures 4 and S3–S5. L.A.O. performed and analyzed all other experiments. L.A.O. wrote the manuscript with input from J.R.C.

DECLARATION OF INTERESTS

The authors declare no competing interests.

Keywords

experience-dependent myelination; oligodendrocyte precursor cell differentiation; dynorphin; stress; striatum; neuropeptide; development; axon selection

INTRODUCTION

Brain plasticity in response to experience is considered essential for learning and memory. Historically, experience-dependent plasticity has been understood to involve changes in synaptic strength (Takeuchi et al., 2014) and structure (Fu and Zuo, 2011), but recent studies have found that non-neuronal cells also respond to experience and can, in turn, regulate neuronal function and behavior (Cheadle et al., 2020; Lacoste et al., 2014; Murphy-Royal et al., 2020; Whiteus et al., 2014; Xin and Chan, 2020).

In particular, the oligodendrocyte lineage can be profoundly impacted by experience (Xin and Chan, 2020). Oligodendrocytes form myelin, the concentrically wrapped membrane that insulates axons and facilitates rapid and efficient action potential conduction. Each oligodendrocyte extends numerous processes to form myelin internodes around many different axons. Oligodendrocytes arise from self-renewing oligodendrocyte precursor cells (OPCs; also commonly referred to as oligodendrocyte progenitor cells or NG2 glia), which populate the entire central nervous system (CNS) and undergo a burst of differentiation and subsequent myelination in development, followed by ongoing – but slowing – OPC differentiation and myelination throughout life (Hill et al., 2018; Hughes et al., 2018; Sturrock, 1980; Wang et al., 2020). This results in the myelination of the axons of some neuronal subtypes while others remain unmyelinated or partially myelinated into adulthood (Call et al., 2021; Micheva et al., 2016; Sturrock, 1980; Tomassy et al., 2014). Recent studies have shown that the experiences of motor, spatial, and contextual learning (Bacmeister et al., 2020; McKenzie et al., 2014; Pan et al., 2020; Steadman et al., 2020; Xiao et al., 2016), socialization (Swire et al., 2019), and sensory stimulation (Hughes et al., 2018) can promote OPC differentiation and myelination. This process, termed experience-dependent myelination, seems to play an important role in learning and memory (McKenzie et al., 2014; Pan et al., 2020; Steadman et al., 2020; Wang et al., 2020; Xiao et al., 2016). Other studies have found that oligodendrocyte lineage cells can be similarly impacted by neuronal activity (Gibson et al., 2014; Mitew et al., 2018), leading to the hypothesis that experience acts on the oligodendrocyte lineage through increases in neuronal activity, likely involving activity-dependent neuronal vesicular release.

To advance our understanding of experience-dependent myelination and the role it plays in brain function and plasticity, there is a need to determine precisely which molecular signals regulate this process. However, to date, no signal has been shown to underlie experience-dependent myelination. We sought to address this question in the context of forced swim stress, an experience involving well-defined signaling pathways and brain regions. We found that forced swim stress induced a pronounced increase in OPC differentiation and myelination in the striatum. Next, we interrogated the mechanisms regulating this novel form of experience-dependent myelination. Acute stress signaling involves several hormones

and neuropeptides, including the neuropeptide family of dynorphin, which contributes to the development or expression of depressive, anxious, and addictive behaviors following acute stress (Knoll and Carlezon, 2010). The dynorphin family of peptides derive from prodynorphin, encoded by *Pdyn* (Schwarzer, 2009). These peptides are stored in large dense-core vesicles (Drake et al., 1994; Yakovleva et al., 2006), and are released from neurons following high levels of neuronal activity (Simmons et al., 1995; Terman et al., 1994; Yakovleva et al., 2006). Crucially, dynorphin peptides (hereafter referred to as dynorphin) are released in the striatum following forced swim stress (Bruchas et al., 2008; Schindler et al., 2012).

We previously performed an unbiased screen for small molecules that promote OPC differentiation and identified a cluster of molecules that activate the endogenous dynorphin receptor, kappa opioid receptor (KOR) (Mei et al., 2016). These results suggest that the endogenous KOR ligand, dynorphin, might play an important role in OPC differentiation and myelination. Taken together, these features of dynorphin – its stress-induced striatal release and its agonism for KOR – led us to investigate its potential role as a novel signal underlying experience-dependent myelination. By genetically or pharmacologically blocking dynorphin-KOR signaling, we abolished striatal stress-induced OPC differentiation, indicating that dynorphin is essential for this novel form of experience-dependent myelination.

Furthermore, we found that dynorphin also promotes developmental OPC differentiation and myelination and demonstrated that this requires the expression of KORs specifically in OPCs. To determine the source of dynorphin, we characterized dynorphin-expressing cells and identified several neuronal subtypes. Using genetic sparse-labeling to trace their axonal projections, we surprisingly found that they were overwhelmingly unmyelinated both under normal conditions and following forced swim stress, in part due to their small size. Collectively, these results identify dynorphin as a novel signal underlying experience-dependent and developmental myelination, whose release from unmyelinated neurons promotes OPC differentiation for the myelination of other axons.

RESULTS

Forced swim stress promotes striatal OPC differentiation in adult mice.

Several recent studies have found that experience can promote OPC differentiation and myelination (Xin and Chan, 2020), but the molecular signals mediating this process remain unresolved. We first sought to determine whether acute stress would promote experience-dependent myelination using the classic paradigm of forced swim stress (Figure 1A).

To assess new OPC differentiation in adult mice, we used *Cspg4*-CreER™; *Mapt*-mGFP mice (Mitew et al., 2018; Wang et al., 2020; Young et al., 2013). *Cspg4* (NG2) is expressed in OPCs, allowing for tamoxifen-dependent recombination in OPCs, while the *Mapt*-mGFP reporter is expressed in oligodendrocytes, preventing mGFP expression until differentiation. Thus, following tamoxifen administration, OPCs that undergo recombination and differentiate can be visualized as mGFP-expressing oligodendrocytes (Figures 1B, 1E, and 1H). Following forced swim stress, we observed a 1.8-fold increase in the

density of mGFP+MBP+ myelinating oligodendrocytes in the striatum (Figures 1C and 1D). By contrast, we observed no change in OPC differentiation in the cortex (Figures 1F and 1G), indicating that forced swim stress induces regionally specific increases in OPC differentiation. These results demonstrate that acute stress can promote striatal OPC differentiation and myelination in a novel form of experience-dependent myelination.

Stress-induced OPC differentiation is dynorphin-dependent.

Since forced swim stress has been shown to cause striatal dynorphin release (Bruchas et al., 2008; Schindler et al., 2012) and activation of the endogenous dynorphin receptor, kappa opioid receptor (KOR), on OPCs promotes their differentiation (Du et al., 2016; Mei et al., 2016), we next investigated whether this experience-dependent myelination in response to acute stress was dependent on dynorphin signaling. To do this, we blocked dynorphin-KOR signaling by two methods. First, we used nor-Binaltorphimine dihydrochloride (nor-BNI), a highly selective, long-acting KOR antagonist that blocks dynorphin signaling (Horan et al., 1992; Portoghese et al., 1987). Nor-BNI blocks KOR agonists from promoting OPC differentiation (Mei et al., 2016) and prevents dynorphin-dependent behavioral outcomes of forced swim stress (McLaughlin et al., 2003). We found that blocking dynorphin-KOR signaling prevented any stress-induced increase in mGFP+MBP+ myelinating oligodendrocytes in the striatum (Figures 2A and 2B), whereas cortical OPC differentiation remained unaltered by forced swim stress (Figures 2C and 2D).

Second, to eliminate dynorphin release, we crossed dynorphin knock-out (*Pdyn* KO) mice to *Cspg4*-CreER™; *Mapt*-mGFP mice to generate *Cspg4*-CreER™; *Mapt*-mGFP; *Pdyn* KO mice. Like with nor-BNI, we found that genetically eliminating dynorphin release prevented any stress-induced increase in striatal mGFP+MBP+ myelinating oligodendrocytes (Figures 2E and 2F), whereas cortical OPC differentiation remained unaffected by forced swim stress (Figures 2G and 2H). Together, these data demonstrate that forced swim stress-induced striatal OPC differentiation and myelination requires dynorphin signaling, identifying dynorphin as a novel signal underlying experience-dependent myelination.

Dynorphin promotes developmental OPC differentiation and myelination.

We next sought to determine whether dynorphin mediates CNS myelination more broadly. We previously observed a deficit in developmental OPC differentiation and myelination in mice lacking KOR in OPCs (henceforth KOR cKO mice) (Mei et al., 2016), suggesting that dynorphin, the endogenous KOR agonist, may promote developmental OPC differentiation and myelination. To test this, we assessed developmental myelination in *Pdyn* KO mice at postnatal day (P) 8. By immunostaining, we observed a 23% decrease in the area occupied by the myelin protein MBP globally across cortex, corpus callosum, and striatum in *Pdyn* KO mice (Figures 3A and 3B). Since we previously showed that activating KOR on OPCs promotes their differentiation (Mei et al., 2016) and we found that dynorphin promotes OPC differentiation following stress (Figures 1 and 2), we hypothesized that the deficit in developmental myelination in *Pdyn* KO mice was due to a decrease in OPC differentiation. Consistent with our hypothesis, we observed a corresponding decrease in the density of oligodendrocytes (CC1+MBP+OLIG2+ cells) in *Pdyn* KO mice at P8 (Figures 3C and 3D) but no change in the density of total oligodendrocyte lineage cells (OLIG2+ cells) (Figures

3C and 3E), indicating a specific deficit in OPC differentiation. Like with KOR cKO mice (Mei et al., 2016), this deficit in OPC differentiation appears to grossly normalize by early adulthood. By 6 wks of age, we observe no difference in the density of oligodendrocytes (ASPA+ cells) between *Pdyn* KO mice and their wild-type littermate controls (Figure S1A and S1B). Together, these results indicate that dynorphin promotes OPC differentiation and myelination in development.

Dynorphin acts through OPC KORs to promote OPC differentiation and myelination.

Our finding that *Pdyn* KO mice phenocopy the developmental deficits in OPC differentiation and myelination observed in KOR cKO mice suggests that dynorphin acts through KORs on OPCs to promote OPC differentiation and myelination. To directly test this hypothesis, we examined whether the deficits in developmental OPC differentiation and myelination induced by *Pdyn* KO mice and KOR cKO mice were additive or redundant. We compared *Pdyn* KO; KOR cKO and KOR cKO littermates at P8. If dynorphin acts independent of OPC KORs to promote developmental OPC differentiation and myelination, we would expect mice lacking both dynorphin and OPC KORs to display a further deficit in developmental myelination than do mice lacking OPC KORs alone. Conversely, if dynorphin acts through OPC KORs to promote OPC differentiation and developmental myelination, the deletion of dynorphin would be redundant with the deletion of OPC KORs and we should observe no difference between these groups. Consistent with the latter hypothesis, we observed no difference in MBP area between *Pdyn* KO; KOR cKO mice and KOR cKO littermates (Figures 3F and 3G). Furthermore, we observed no difference in the density of oligodendrocytes (CC1+MBP+OLIG2+ cells) (Figures 3H and 3I) or total oligodendrocyte lineage cells (OLIG2+ cells) (Figures 3H and 3J). Together, these data indicate that dynorphin acts through OPC KORs to induce OPC differentiation and myelination.

Dynorphin is expressed in a subset of neurons.

As the activity of multiple different neuronal subtypes has been implicated in regulating OPC differentiation and myelination (Gibson et al., 2014; Mitew et al., 2018), we sought to identify the neuronal subtypes expressing dynorphin. To visualize dynorphin-expressing cells, we utilized *Pdyn*-Cre; nTnG and *Pdyn*-Cre; mTmG mice, where nuclear EGFP and membrane EGFP expression, respectively, are driven by Cre. In *Pdyn*-Cre; nTnG mice, we observed widespread EGFP+ nuclei in the striatum and cortex (Figure 4A). The cortical EGFP+ nuclei were distributed into two populations. One population was tightly clustered in upper layer II/III (Figures 4A and 4C). The other population was more broadly distributed in the deeper cortical layers, with the majority in layer V and some in the deeper part of layers II-IV or in layer VI (Figures 4A, 4C, and 4D). The striatal EGFP+ nuclei were distributed throughout the striatum and in clusters of higher density (Figure 4A, S2A–S2C). In *Pdyn*-Cre; mTmG mice, the distribution of dynorphin-expressing cells observed in *Pdyn*-Cre; nTnG mice was replicated and, furthermore, the their processes could be visualized (Figure 4B). Tracts of mEGFP+ axons projecting towards or away from (Figure 4E) and within (Figure 4F) the corpus callosum could be observed, as well as mEGFP+ axons elaborating in layer I (Figure 4G) and projecting in striatal axon bundles (Figure 4H).

To identify the cell types expressing dynorphin, we examined colocalization of EGFP+ nuclei in *Pdyn*-Cre; nTnG mice with various markers. We did not observe any colocalization with glial markers (Figures S3A–S3D). The upper layer II/III EGFP+ nuclei colocalized with pyramidal neuron markers CUX1 and CaMKIIa (Figures 4I–4K) and rarely colocalized with interneuron markers (Figures 4K and S4A–S4F), indicating that this population is made up of layer II/III pyramidal neurons, which project through the corpus callosum (Figures 4E–4F) to innervate the contralateral cortex. The EGFP+ nuclei in the deeper cortical layers primarily colocalized with somatostatin (SST) and reelin, and to a much lesser extent calbindin and calretinin (Figures 4L–4N and S5A–S5F), in agreement with a previous report (Sohn et al., 2014). This molecular profile is suggestive of Martinotti cells, interneurons predominantly localized to layer V but also found in layers II/III and VI, which project their axons into layer I (Tremblay et al., 2016). These deeper cortical population matched this cortical distribution (Figures 4A, 4C, and 4D) and their mEGFP+ axonal ramifications were observable throughout layer I (Figure 4G), indicating these cells are indeed Martinotti cells. Finally, all EGFP+ nuclei in the striatum colocalized with CTIP2 (Figure 4O–4Q), a marker for medium spiny neurons, as striatal dynorphin-expressing neurons are known to be direct-pathway medium spiny neurons (Gerfen et al., 1990). Collectively, these results identify three populations of dynorphin-expressing neurons throughout the cortex and striatum.

Axons of dynorphin-expressing neurons are unmyelinated.

Not all axons in the brain are myelinated and many axons are only partially myelinated (Call et al., 2021; Micheva et al., 2016; Sturrock, 1980; Tomassy et al., 2014), but how axons are selected for myelination remains an outstanding question. A recent study showed that increased activity of layer II/III pyramidal neurons promotes OPC differentiation and myelination as well as the targeting of this new myelin to those activated pyramidal axons (Mitew et al., 2018). However, it is unknown which signaling mechanisms regulate this process, and whether the same axonal signal could both promote OPC differentiation and targeting of the resulting myelin to the source axon. Other studies have shown that the selection of axons for myelination is promoted by neuronal vesicular release (Hines et al., 2015; Koudelka et al., 2016). These findings led us to ask whether dynorphin, in addition to its role in promoting OPC differentiation, could also promote the selection of dynorphin-expressing neurons for myelination. To test this possibility, we examined whether the axons of dynorphin-expressing neurons were myelinated. The high density of mEGFP+ axons throughout the brain (Figures 4B and 4E–4H) impeded our ability to distinguish individual axons in *Pdyn*-Cre; mTmG mice by immunofluorescence. Therefore, we used a novel method for sparsely labeling cells: the STARS (stochastic gene activation with regulated sparseness) reporter mouse. A single copy of the STARS transgene allows for membrane EYFP (mEYFP) expression in only 10% of Cre-expressing cells (Ibrahim et al., 2018). Using *Pdyn*-Cre; STARS mice, we were able to assess the myelination status of individual axons of dynorphin-expressing neurons in several regions using confocal microscopy (Figures 5A, 5C, 5E, and S6). Looking for colocalization of mEYFP+ axons and MBP+ myelin, we found that the axons of dynorphin-expressing neurons were overwhelmingly unmyelinated in all regions observed (Figures 5A–5F, and S6). The axons of dynorphin-expressing layer II/III pyramidal neurons were unmyelinated in cortical layer VI (99.76%; Figures 5A and 5B) and in the corpus callosum (Figure S6). The axons of dynorphin-

expressing Martinotti cells were unmyelinated in cortical layer I (100%; Figures 5C and 5D). Finally, in the striatum, axons of dynorphin-expressing neurons were unmyelinated in the neuropil (gray matter: 99.40%) and axon tracts (white matter: 95.01%; Figures 5E and 5F). Together, these data indicate that dynorphin does not promote the myelination of dynorphin-expressing axons over the course of normal development.

Dynorphin-expressing neurons remain unmyelinated following forced swim stress.

Although the axons of dynorphin-expressing neurons were unmyelinated at baseline, we hypothesized that an experience like forced swim stress, which induces dynorphin release (Bruchas et al., 2008; Schindler et al., 2012) and increases striatal OPC differentiation (Figures 1 and 2), could promote their myelination in the striatum. To test this hypothesis, we put *Pdyn*-Cre; STARS mice through our forced swim stress paradigm (Figures 1A and 5G). We found that forced swim stress did not alter the percentage of unmyelinated mEYFP+ axons in the gray matter (Figures 5H and 5J) or white matter of the striatum (Figures 5I and 5J). These results indicate that following forced swim stress – like at baseline – dynorphin does not promote the myelination of dynorphin-expressing axons.

Small axonal diameters contribute to low myelination rates of dynorphin-expressing neurons.

Axons smaller than roughly 0.3 μm in diameter are unable to be myelinated by oligodendrocytes (Lee et al., 2012) and previous work has shown that cortical SST+ Martinotti cells – a subset of which express dynorphin (Figures 4L–4N) – are unmyelinated due to their small axonal diameters (Stedehouder et al., 2019). This led us to interrogate whether the axons of dynorphin-expressing neurons may remain unmyelinated due to size. We estimated axon diameters of mEYFP+ dynorphin-expressing neurons by measuring the full-width at half maximum (FWHM) of mEYFP fluorescence intensity across axons (Figure 6A), as previously described (Call and Bergles, 2021; Stedehouder et al., 2019). In all regions, a substantial percentage of unmyelinated mEYFP+ axons were below 0.3 μm in diameter (cortical layer VI: 38.19%; cortical layer I: 45.12%; striatal GM: 46.15%; striatal WM: 22.09%) and the vast majority were below 0.4 μm in diameter (cortical layer VI: 89.60%; cortical layer I: 92.61%; striatal GM: 90.83%; striatal WM: 81.35%) (Figures 6C–6F). By comparison, the diameters of the myelinated axons in these same regions, as measured from electron micrographs (Figure 6B), were substantially larger (above 0.4 μm in diameter: cortical layer VI: 85.11%; cortical layer I: 92.79%; striatal WM: 84.40%) (Figures 6C–6E).

We also measured the diameters of the few mEYFP+ axons of dynorphin-expressing neurons that were myelinated (Figure 6A). On average, we found that myelinated mEYFP+ axons were larger than unmyelinated mEYFP+ axons in all regions where we observed mEYFP+ axon myelination (Figures 6C, 6E, and 6F). When considering only suprathreshold axons, diameter still influenced myelination status. mEYFP+ axons larger than 0.5 μm had substantially higher rates of myelination (cortical layer VI: 10.71%; striatal GM: 22.47%; striatal WM: 54.22%) than those between 0.3 μm and 0.5 μm (cortical layer VI: 0.62%; striatal GM: 0.94%; striatal WM: 2.48%). Together, these data indicate that small axon size indeed contributes to the extremely low myelination rate of dynorphin-expressing neurons.

However, small axonal diameter does not entirely account for the low myelination rate of dynorphin-expressing neurons. Even when compared across the same axon size, the myelination rate of dynorphin-expressing neurons is substantially lower than that of some other CNS neuronal subtypes. Below 0.5 μm, the axons of dynorphin-expressing neurons are almost entirely unmyelinated (cortical layer VI: 0.38%; cortical layer I: 0%; striatal GM: 0.50%; striatal WM: 1.91%), while parvalbumin neurons and thalamocortically projecting ventral medial nucleus neurons in cortical layer I are myelinated at rates of 30% and 21%, respectively (Call and Bergles, 2021). Clearly – in addition to small axonal diameter – there are other, yet to be defined factors that also contribute to preventing the myelination of dynorphin-expressing neurons.

DISCUSSION

Overall, we identify the neuropeptide dynorphin as a neuronal signal promoting experience-dependent OPC differentiation and myelination following acute stress (Figures 1 and 2). Dynorphin also promotes developmental OPC differentiation and myelination (Figures 3A–3E) and exerts its pro-differentiation effects by acting on OPC KORs (Figures 3F–3J). Intriguingly, we found that the axons of dynorphin-expressing neurons are unmyelinated both under normal conditions (Figures 5A–5F and S6) and following acute stress (Figures 5H–5J), which can be partially attributed to their small size (Figures 6C–6F). Based on our findings, we propose the following model wherein unmyelinated, dynorphin-expressing neurons promote the myelination of neighboring axons during development and following acutely stressful experiences by releasing dynorphin to induce OPC differentiation (Figure 7).

Experience can promote OPC differentiation and myelination (Bacmeister et al., 2020; Hughes et al., 2018; McKenzie et al., 2014; Pan et al., 2020; Steadman et al., 2020; Swire et al., 2019; Xiao et al., 2016), but until now, no signal has been found to underlie this process. The discovery of neuronal glutamatergic and GABAergic synaptic input onto OPCs two decades ago (Bergles et al., 2000; Lin and Bergles, 2003) provided a compelling avenue: neurons could convey changes in experience by altering their synaptic input onto OPCs to induce OPC differentiation. Consequently, much of the focus has been on how these neurotransmitters act on OPCs through their ionotropic receptors. Our study, which identifies a neuropeptide as a neuronal signal underlying experience-dependent OPC differentiation and myelination (Figures 1 and 2), suggests a broader approach is necessary. Dynorphin may play a similar role in promoting OPC differentiation and myelination in other experiences involving dynorphin release, such as other stressors, during the development of neuropathic pain, and following repeated drug exposure (Knoll and Carlezon, 2010). However, dynorphin is likely only one of several signals mediating the myriad of responses of oligodendrocyte lineage cells to different experiences. Beyond promoting OPC differentiation and myelination, experience can also alter OPC proliferation (McKenzie et al., 2014; Pan et al., 2020; Steadman et al., 2020), myelin thickness (Liu et al., 2012; Makinodan et al., 2012), oligodendrocyte complexity (Makinodan et al., 2012; Swire et al., 2019), node and internode structure (Cullen et al., 2021; Etxeberria et al., 2016; Yang et al., 2020) and new internode formation (Bacmeister et al., 2020). We propose that

investigation into other signals regulating these processes should consider molecules beyond the classical fast-acting neurotransmitters.

Neuropeptides and neurotrophins are attractive candidates for regulating experience-dependent plasticity in the oligodendrocyte lineage. They bind G-protein coupled receptors (GPCRs) – like kappa opioid receptor – and receptor tyrosine kinases (RTKs), respectively, providing great opportunity to affect the intracellular signaling and gene expression machinery involved in experience-dependent myelination. Indeed, several ligands of GPCRs and RTKs can mediate OPC proliferation and differentiation (Bergles and Richardson, 2016) and these receptors are upstream of the ERK/MAPK and PI3K/Akt/mTOR signaling cascades that control myelin thickness (Goebbels et al., 2010; Jeffries et al., 2016) and other pathways regulating oligodendrocyte complexity (Czopka et al., 2013; Swire et al., 2019). Furthermore, neuropeptides and neurotrophins are stored in large dense-core vesicles and released in response to high levels of neuronal activity, providing a means by which neurons could signal changes in experience to oligodendrocyte lineage cells. A recent study found optogenetic stimulation of layer V pyramidal neurons acts via the neurotrophin BDNF to alter oligodendrocyte lineage cells (Geraghty et al., 2019). Might BDNF promote experience-dependent myelination in BDNF-associated learning and memory tasks (Bekinschtein et al., 2014)? And yet, direct activity-dependent release from neurons is not necessary for candidate ligands if their expression or release is modulated by experience through other means. Two other studies have implicated neuregulin 1 type III and endothelin-1 and/or 3 in the deficits in oligodendrocyte complexity and social behavior observed in socially isolated mice. The mRNA for these ligands decreased following social isolation and disruption of their respective receptors, ErbB3 (an RTK) in oligodendrocytes or endothelin receptor EDNRB (a GPCR) in OPCs, phenocopied the social isolation-induced deficits in oligodendrocyte complexity and social behavior (Makinodan et al., 2012; Swire et al., 2019). We anticipate that future studies into these and other GPCR and RTK ligands will uncover many more signals regulating experience-dependent myelination.

An interesting regional distinction arose in our findings between developmental and experience-dependent myelination. We observed a role for dynorphin in promoting experience-dependent OPC differentiation in the striatum but not in the cortex (Figures 1 and 2), while in development dynorphin promotes OPC differentiation and myelination in both regions (Figure 3A–3E). Possibly, cortical OPCs lose KOR expression or are otherwise unresponsive to KOR activation following early development. Alternatively, this distinction may be explained by regional differences in forced swim stress-induced dynorphin release between the striatum, where forced swim stress has been well documented to induce dynorphin release (Bruchas et al., 2008; Schindler et al., 2012), and the cortex. To distinguish between these possibilities, we tested whether KOR activation could promote cortical OPC differentiation outside of early development. We treated P30 wild-type mice systemically with the highly selective KOR agonist (±)-U-50488 (Von Voigtlander et al., 1983) (Figure S7A) and found that it increased cortical oligodendrocyte density (Figure S7B and S7C). These data indicate that cortical OPCs maintain the capacity to differentiate in response to KOR activation beyond early development, suggesting that the lack of cortical OPC differentiation in response to forced swim stress may be due to differential dynorphin release between regions.

Timely myelination of the appropriate axons to facilitate learning and memory or otherwise advantage an organism requires the precise coordination of signals regulating new oligodendrocyte formation and the selection of which axons they will myelinate during their typically short period of myelin formation following differentiation (Bacmeister et al., 2020; Czopka et al., 2013). Neuronal control of OPC differentiation and axon selection dramatically simplifies this coordination – the axons that require additional myelination could both promote OPC differentiation and their own subsequent myelination, perhaps even using the same molecular signal to regulate both processes. Considering this, we were somewhat surprised to discover that the axons of dynorphin-expressing neurons are overwhelmingly unmyelinated (Figures 5A–5F and S6). These findings instead support a model wherein dynorphin release from unmyelinated, dynorphin-expressing neurons acts as a diffuse OPC differentiation signal to promote the myelination of neighboring axons, which are selected for myelination through alternate means (Figure 7). How, then, in instances where the myelin demand of certain axons increases in response to experience, could dynorphin-expressing neurons coordinate dynorphin release with the presence of axon selection cues in these axons? One possibility is through shared input to both neurons. For example, in cortical layer II/III, unmyelinated dynorphin-expressing pyramidal neurons are interspersed with myelinated non-dynorphin-expressing pyramidal neurons (Figures 4I–4J) whose myelination is promoted by layer II/III pyramidal neuron activity (Mitew et al., 2018). Shared inputs to activate these dynorphin- and non-dynorphin-expressing populations could coordinate the release of dynorphin to promote OPC differentiation and the expression of an axon selection cue in adjacent non-dynorphin-expressing axons to promote their selection for myelination.

Our observation that the axons of dynorphin-expressing neurons are almost entirely unmyelinated (Figures 5A–5F and S6) raises two other important questions. First, considering this complication of coordination, why would axons not destined for myelination regulate the myelination process? One reason might be to preserve the ability of dynorphin-expressing neurons to promote OPC differentiation and myelination over time. Myelin coverage could obstruct axonal dynorphin release sites, so unmyelinated dynorphin-expressing axons would retain their ability to promote OPC differentiation and myelination in response to stress or other experiences throughout life.

Second, how do dynorphin neurons prevent the myelination of their axons? Here, we show that their small axonal diameter is a contributing factor but does not fully explain their lack of myelination (Figure 6). Likely, axons of dynorphin-expressing neurons are equipped with molecular factors that negatively regulate their myelination and/or they lack factors to positively promote their myelination. Might dynorphin itself be a negative factor preventing the myelination of dynorphin-expressing neurons? Consistent with this hypothesis, in addition to its axonal release, dynorphin is also frequently released from dendrites (Drake et al., 1994; Simmons et al., 1995; Yakovleva et al., 2006) – another structure not targeted for myelination. However, dynorphin appears to be a poor candidate to either negatively or positively regulate the selection of structures for myelination. Such cues should be precisely localized to the structure of interest. This can be readily achieved by membrane-bound adhesion molecules or through neurotransmitter release at axon-OPC synapses (Osso and Chan, 2017). By contrast, dynorphin’s release has poor spatial resolution; unlike with

classical neurotransmitters, it is often released extrasynaptically from axons (Drake et al., 1994) and there are no specialized reuptake channels localized to these sites to prevent its diffusion. More likely, dynorphin-expressing neurons use other currently undefined cues to prevent their myelination. Ultimately, the objective is to understand how such negative and positive axon selection cues coordinate with differentiation signals like dynorphin to promote the myelination of specific axons during experience-dependent myelination, and to elucidate how this process alters behavioral outcomes.

STAR METHODS

RESOURCE AVAILABILITY

Lead Contact—Further information and requests for resources and reagents should be directed to and will be fulfilled by the Lead Contact, Jonah Chan (jonah.chan@ucsf.edu).

Materials Availability—This study did not generate new unique reagents.

Data and Code Availability—The data supporting this study is available from the corresponding author upon reasonable request.

EXPERIMENTAL MODEL AND SUBJECT DETAILS

All mice were handled in accordance with the approval of the University of California, San Francisco Administrative Panel on Laboratory Animal Care and group housed under standard barrier conditions in the Laboratory Animal Research Center (LARC) in the Sandler Neurosciences Center at UCSF, Mission Bay. Mice were given food and water ad libitum and were on a 12 h light/dark cycle. Both females and males were used for all experimental conditions. For forced swim stress experiments, *Cspg4*-CreER™ BAC transgenic mice (Zhu et al., 2011) were generously provided by Dr. Anders Persson (University of California, San Francisco; also available from Jackson Laboratory, Stock No. 008538). *Mapt*-mGFP knock-in mice (Hippenmeyer et al., 2005) were generously provided by Dr. John Rubenstein (University of California, San Francisco; also available from Jackson Laboratory, Stock No. 021162). These lines were crossed to generate *Cspg4*-CreER™ /+; *Mapt*-loxP-STOP-loxP-mGFP/loxP-STOP-loxP-mGFP mice. *Pdyn* knock-out mice (Sharifi et al., 2001) were generously provided by Dr. Michael Bruchas (University of Washington; also available from Jackson Laboratory, Stock No. 004272) as homozygotes. For forced swim stress experiments in *Pdyn* KO mice, *Pdyn* KO mice were crossed into *Cspg4*-CreER™ and *Mapt*-mGFP mice to generate *Cspg4*-CreER™/+; *Mapt*-loxP-STOP-loxP-mGFP/loxP-STOP-loxP-mGFP; *Pdyn* −/− mice. 12–16 week old littermates of the same genotype underwent forced swim stress or served as controls. To compare developmental OPC differentiation and myelination, *Pdyn* KO mice were crossed with wild-type C57BL/6J mice (Jackson Laboratory, Stock No: 000664) to generate *Pdyn* +/− mice for breeding to generate *Pdyn* −/− and *Pdyn* +/+ littermates, which were analyzed for developmental myelination at postnatal day (P) 8. KOR floxed (*Oprk1*-loxP) mice (Chefer et al., 2013) were generated and generously provided by Dr. Jennifer Whistler (University of California, Davis). *Olig2*-Cre mice (Schüller et al., 2008) were generously provided by Dr. David Rowitch (University of California, San Francisco; also available from Jackson

Laboratory, Stock No. 011103). They were crossed with *Pdyn* KO mice to generate *Pdyn* +/−; *Olig2*-Cre/+; *Oprk1*-loxP/loxP mice and *Pdyn* +/−; *Oprk1*-loxP/loxP mice for breeding to generate *Pdyn* −/−; *Olig2*-Cre/+; *Oprk1*-loxP/loxP mice and *Pdyn* +/+; *Olig2*-Cre/+; *Oprk1*-loxP/loxP littermates for developmental myelination analysis at P8. *Pdyn*-Cre knock-in mice (Krashes et al., 2014) (Stock No. 027958) and mTmG mice (Muzumdar et al., 2007) (Stock No. 007676) were obtained from Jackson Laboratory as homozygotes. nTnG mice (Prigge et al., 2013) were generously provided by Dr. Samuel Pleasure (University of California, San Francisco; also available from Jackson Laboratory, Stock No. 023537) as homozygotes. Pdyn-Cre mice were bred to nTnG mice and mTmG mice to generate *Pdyn*-Cre/+; Rosa26-loxP-ntdTomato-loxP-nEGFP/+ mice and *Pdyn*-Cre/+; Rosa26-loxP-mtdTomato-loxP-mEGFP/+, which were analyzed for reporter expression at 12–16 weeks. STARS reporter mice (Ibrahim et al., 2018) were generated and generously provided by Dr. Li Zhang (University of Southern California; also available from Jackson Laboratory, Stock No. 032453) as heterozygous animals. They were crossed with wild-type C57BL/6J mice (Jackson Laboratory, Stock No: 000664) to establish a colony. They were then bred to *Pdyn*-Cre mice to generate *Pdyn*-Cre/+; Rosa26-lox3172-mCherry-loxP-lox3172-mEYFP-loxP/+ mice, which were analyzed for dynorphin axon myelination at 12–16 weeks. Detailed identification of mouse lines can be found in the Key Resources Table. Genotypes were determined by PCR amplification and visualization with 0.0005 % ethidium bromide (BioRad, Cat. No. 161–0433) on a 2% agarose (Fisher Scientific, Cat. No. BP160–100, in 1X TAE, Fisher Scientific, Cat. No. 50–103-5139) gel. Primers and amplified fragment sizes are listed in Table S1.

METHOD DETAILS

Forced swim stress—Forced swim stress was performed in 12–16 week old mice as previously described (McLaughlin et al., 2003). Both experimental mice and controls were brought in their home cage to the behavior room 1 h prior to swim. Experimental mice were placed in an opaque 5 gallon (28.5 cm diameter, 37 cm tall) bucket filled to a depth of 20 cm with 30 °C tap water to swim without the opportunity to escape. After each trial, mice were dried with paper towel and returned to their home cage. Control mice remained in the home cage. On the first day, experimental mice swam for a single trial of 15 min. On the second day, experimental mice swam for four trials of 6 min each, each separated by 7 min in their home cage. All mice were returned to the mouse facility within 10 min of the final swim on both days.

Drug administration—Tamoxifen (Sigma-Aldrich, Cat. No. T5648) was stored as a powder at 4 °C protected from light. On the day of administration, tamoxifen was weighed and dissolved in peanut oil to a concentration of 1 mg/mL. The solution was shaken at 1000rpm at 42 °C for several hours until tamoxifen had dissolved. Forced swim stressed mice and littermate controls were administered 60 μL of solution by oral gavage three days prior to the first forced swim stress trial. nor-Binaltorphimine dihydrochloride (nor-BNI, Sigma-Aldrich, Cat. No. N1771) was stored as a powder at −20 °C. On the day of administration, nor-BNI was weighed and dissolved in autoclaved phosphate buffered saline (PBS, in Milli-Q Synthesis A10 purified water, pH 7.4) to a concentration of 1 mg/mL. The solution was shaken at 1000rpm at room temperature (RT) for 20 min until

nor-BNI had dissolved, and then filtered through a 0.22 μm filter (EMD Millipore, Cat. No. SLGP033RS). As previously described, the solution was administered by intraperitoneal injection at 10 mg/kg to both experimental and control animals 1 h prior to the first swim trial on both days of forced swim stress sessions (McLaughlin et al., 2003). (±)-U-50488 (Tocris, Cat. No. 0495) was stored as a powder at RT. On the day of administration, it was weighed and dissolved to 1mg/mL in water. The solution was shaken at 1000rpm at RT for 20 min until (±)-U-50488 had dissolved. The (±)-U-50488 solution or water were administered by gavage at 10mg/kg, as previously described (Mei et al., 2016), to wild-type littermates once a day starting at P30 for four consecutive days (P30-P33).

Tissue processing and immunohistochemistry—Mice were deeply anesthetized with intraperitoneal injection of 2,2,2-tribromoethyl alcohol (Sigma-Aldrich, Cat. No. T48402) and perfused transcardially with 1X PBS followed by 4% paraformaldehyde (PFA, Electron Microscopy Sciences, Cat. No. 19210 in PBS, pH 7.4). Brains were immediately dissected from the skull and post-fixed in 4% PFA at 4 °C for 2 h (for immunostaining for ASPA (EMD Millipore), CD140a, PV, calretinin, and calbindin, as well as GFP when used in the same sections) or overnight (all other immunostaining). Brains were rinsed with 1X PBS + 0.02% sodium azide (BioExpress, Cat. No. 0639) and transferred to 30% sucrose (Sigma-Aldrich, Cat. No. S9378) + 0.02% sodium azide (in PBS) solution for cryoprotection until sinking (~24–48 h at 4 °C). Brains were mounted with a 2:1 30% sucrose:optimum cutting temperature solution (OCT, Tissue-Tek, Cat. No. 4583) to a freezing stage (Thermo Fisher Scientific, KS 34) and cryosectioned using a sliding microtome (Thermo Fisher Scientific, HM 450) coronally at 30 μm thickness. Sections for CaMKIIa immunostaining were 14 μm to allow for penetration of the CaMKIIa antibody through the entire tissue. Sections for analysis of mEYFP+ axon myelination were 6 μm to allow for penetration of the MBP antibody into dense white matter tracts. Floating sections were stored in 1X PBS + 0.02% sodium azide at 4 °C until immunostaining. For immunostaining, floating sections were blocked and permeabilized in 20% normal goat serum (NGS, Sigma-Aldrich, Cat. No. G9023) + 0.2% Triton X-100 (Sigma-Aldrich, Cat. No. T8787, in DPBS with calcium, magnesium, Thermo Fisher Scientific, Cat. No. 14040133) for 2 h shaking at 80 rpm at RT. Sections were then incubated in primary antibodies diluted in fresh blocking solution overnight (two overnights for CaMKIIa immunostaining) shaking at 55 rpm at 4 °C. Primary antibodies and their dilutions are listed in the Key Resources Table. Sections were washed in PBS for 30 min shaking at 80 rpm at RT and then incubated in secondary antibodies diluted in 20% NGS for 1 h shaking at 80 rpm at RT. Secondary antibodies and their dilutions were as follows: AlexaFluor 488-, AlexaFluor 594-, and AlexaFluor 647-conjugated goat antibodies to rat, rabbit, mouse, and chicken (1:1000, Thermo Fisher Scientific, Cat. Nos. A-21245, A-11034, A-11007, A-21236, A-21247, A-11039). To prevent cross-reaction when rat and mouse primary antibodies were used in the same sections, secondary antibodies from Jackson ImmunoResearch were used (1:800, Cat. Nos. 115–545-166, 112–585-167). For sections with goat primary antibody, 10% normal donkey serum (NDS, Sigma-Aldrich, Cat. No. D9663, in DPBS with calcium, magnesium) was used in place of 20% NGS for all steps; secondary antibodies were donkey (Thermo Fisher Scientific, Cat Nos. A-21206, A-21447). DAPI (40ng/ml, Thermo Fisher Scientific, Cat No. D1306) was added for the last 8 min of secondary antibody incubation. Sections were then washed in PBS for 30min

shaking at 80 rpm at RT, mounted onto Superfrost Plus microscope slides (Thermo Fisher Scientific, Cat. No. 12–550-15), dried, rinsed in water, and dried again. Slides were then coverslipped (Thermo Fisher Scientific, Cat. No. 12–543C) using Glycergel Mounting Medium (Agilent, Cat. No. C0563) for imaging. Antigen retrieval was required for CaMKIIa and ASPA (GeneTex) immunostaining. Prior to blocking, floating sections were washed in PBS and incubated for 7 min in L.A.B. Solution (Polysciences, Cat No. 24310–500) then washed again in PBS shaking at 80 rpm at RT. To adequately visualize individual myelin sheaths with MBP immunostaining in densely myelinated regions for analysis of mEFYP+ axon myelination, prior to blocking, floating sections were dipped in water, then dehydrated and rehydrated using ascending then descending ethanol (Sigma-Aldrich, Cat. No. E7023) dilutions (50, 70, 90, 95, 100, 95, 90, 70, 50% in water) for 2 min each shaking at 80 rpm at RT as previously described (Duncan et al., 2018), then dipped in water again, and finally washed in PBS until blocking.

Image acquisition—All analysis was centered around Bregma 0.9 mm. To compare OPC differentiation in forced swim stress mice and controls, in each mouse, every fifth section from Bregma 1.5 mm to Bregma 0.3 mm was immunostained, for a total of eight 30 μm coronal sections centered around Bregma 0.9mm. Tiled z stacks of each full section were taken using a Zeiss Axio Scan Z1 Slide Scanner at 20X. The same imaging settings were used for all images across all experimental replicates. For presentation in figures to improve contrast of mGFP and MBP staining against the background and for higher magnification images, representative images were taken using a Zeiss LSM 700 laser scanning confocal microscope. To compare developmental OPC differentiation and myelination, in each mouse, five consecutive 30 μm coronal sections centered around Bregma 0.9 mm were immunostained. Immunofluorescent images were acquired on a Zeiss Axio Imager M2 with a Zeiss AxioCam MRm and Zeiss Apotome 2. The same imaging settings were used for all mice within an experimental replicate. For MBP area, 3–4 tiled 10X z stack images encompassing the entire region shown in Figure 3A and 3F were taken per mouse. Only one hemisphere per section was imaged. For CC1+MBP+OLIG2+ and OLIG2+ cell quantification, both hemispheres were imaged if possible and a total of 7–10 tiled 10X z stack images encompassing the region shown in Figure 3C and 3H were taken per mouse. To compare ASPA+ oligodendrocyte density in adult mice, every other section (five total) centered around Bregma 0.9 mm were immunostained. Immunofluorescent images were acquired using a Zeiss LSM 700 laser scanning confocal microscope. The same imaging settings were used for all mice within an experimental replicate. Both hemispheres were imaged if possible and a total of 7–9 tiled 20X z stack images encompassing the region shown in Figure S1A and Figure S7B were taken per mouse. For analysis of dynorphin reporter expression, consecutive 30 μm coronal sections centered around Bregma 0.9mm were immunostained for EGFP and several neuronal and glial markers. Sections immunostained for CaMKIIa were 14 μm (see “Tissue processing and immunohistochemistry”). For quantification of colocalization of nEGFP with each neuronal marker, two sections were imaged per mouse in each brain region using a Zeiss LSM 700 laser scanning confocal microscope. Per section, one tiled 20X z stack image encompassing all EGFP+ cells in the isocortex of one hemisphere, excluding the medial region, was taken. In dorsal and ventral striatum, one tiled image of four and two 20X z

stack tiles were taken per section, respectively. For analysis of mEYFP+ axon myelination and diameters, consecutive 6 μm coronal sections centered around Bregma 0.9mm were imaged using a Zeiss LSM 700 laser scanning confocal microscope. Six individual 63X z stack images were taken per mouse (3 per section, 2 sections per mouse) in medial cortical layer VI, lateral cortical layer I, and distributed throughout dorsal striatum.

Electron microscopy—Mice were perfused transcardially with 0.1M sodium cacodylate (Electron Microscopy Sciences, Cat. No. 12300) followed by 1.2% glutaraldehyde (Electron Microscopy Sciences, Cat. No. 16220) 2% paraformaldehyde (Electron Microscopy Sciences, Cat. No. 15710) in 0.1M sodium cacodylate, pH 7.4. Brains were immediately dissected from the skull and post-fixed in 1.2% glutaraldehyde 2% paraformaldehyde in 0.1M sodium cacodylate, pH 7.4 at 4 °C for 1 wk. Brains were transferred to 30% sucrose + 0.02% sodium azide (in PBS) solution for cryoprotection until sinking. Brains were mounted with a 2:1 30% sucrose:optimum cutting temperature solution to a freezing stage and cryosectioned using a sliding microtome at 500 μm thickness. Regions of interest were then micro-dissected from 500 μm sections and returned to 1.2% glutaraldehyde 2% paraformaldehyde in 0.1M sodium cacodylate, pH 7.4 at 4 °C and transferred to the Cell Imaging Lab at the San Francisco Veterans Affairs Medical Center. There, the samples were rinsed with 0.1M sodium cacodylate, pH 7.4 and post-fixed and stained with 2% osmium tetroxide and stained with 5% uranyl acetate (Electron Microscopy Sciences). The samples were then dehydrated with ethanol, cleared with propylene oxide, and embedded in Eponate 12 Resin (Ted Pella). Sections were cut using a Leica EM UC7 Ultramicrotome, oriented such that axons in the same orientation as axons of dynorphin-expressing neurons were cut in cross-section. Images were acquired using a Philips Tecnai 10 Electron Microscope with a SIA-16M camera.

QUANTIFICATION AND STATISTICAL ANALYSIS

Image blinding and analysis—In forced swim stress experiments, quantification was performed with Fiji software (NIH) using stacks of 10 individual z planes to allow for unambiguous identification of the soma of mGFP+MBP+ cells (by colocalization with DAPI). Images were randomized and blinded using a Java program written by L.A.O. prior to any analysis. All mGFP+MBP+ somas were quantified in the entire isocortex and striatum (caudoputamen and nucleus accumbens) of all sections. Density per section was determined by dividing the number of mGFP+MBP+ cells by the area of the region of interest, which was manually delineated using landmarks defined by DAPI and MBP. In each mouse, this value was averaged across all sections to provide the average cell density per mouse, which was then normalized to the control average per cohort. To analyze MBP+ area and CC1+MBP+Ol2+, OLIG2+, and ASPA+ cell density, maximum intensity projections of z stacks were analyzed using Fiji software. Images were randomized and blinded using a Java program written by L.A.O. prior to any analysis. Regions for analysis were standardized using the same ROI for all images, which was positioned based on brain landmarks defined by DAPI. MBP area was measured as the area of pixels above a standardized threshold intensity. CC1+MBP+OLIG2+, OLIG2+, and ASPA+ cell counts were performed manually and were divided by the area of the region of interest. In each mouse, quantification from all images was averaged, and that average was then normalized to the control average per litter.

For quantification of colocalization of dynorphin-expressing EGFP+ nuclei with neuronal markers, maximum intensity projections of z stacks were analyzed using either Fiji or Imaris 9.3.0 software (Bitplane). Using Fiji, quantification was performed manually. Using Imaris, quantification was performed using the Surfaces tool and verified manually. All EGFP+ nuclei within the imaged regions were quantified. The delineation between upper and deeper cortical layer cells was performed based on localization in the cortex using the EGFP+ channel and DAPI without looking at colocalization with neuronal markers. Quantification of mEYFP+ axon myelination was performed with Fiji using a stack of the maximum intensity z projection and each individual z plane for an image. mEYFP+ segments were traced with the Freehand Line tool and added the ROI Manager. Panning through individual z planes allowed for accurate tracing of overlapping mEYFP+ segments. To determine if mEYFP+ segments were myelinated, colocalization with MBP immunostaining was examined across z planes. mEYFP+ dendrites were readily identifiable in all regions by their larger diameter and the presence of spines; they excluded from quantification. To compare mEYFP+ segment myelination in control and forced swim stressed mice, images were first randomized and blinded using a Java program written by L.A.O. prior to any analysis. Quantification of mEYFP+ axon diameter was performed on half of the images used for percentage myelination quantification (three 63X confocal images per region per mouse). Maximum intensity z projection images with annotated unmyelinated and myelinated axons were opened in Fiji. The mEYFP fluorescent intensity was averaged across a 1 μm length of axon by drawing a line (with 1 μm thickness; blue in Figure 6A) transecting the axon in a representative linear region and using the “Plot Profile” tool. Only axons with linear regions ≥ 1 μm unobstructed by other mEYFP+ axons were used. Then, a Gaussian curve was fit to the distribution. Axons were only included if $R^2 > 0.90$. The full width at half maximum (FWHM) was calculated from the standard deviation ($d = 2\sigma\sqrt{2\ln 2}$) of the Gaussian curve and used as the estimate for that axon’s diameter (Figure 6A). With these parameters, we were able to quantify the diameters of 39.62% of mEYFP+ axons in cortical layer VI, 45.34% in cortical layer I, 47.69% in striatal GM, and 55.32% in striatal WM of the images analyzed. Quantification of the diameters of overall myelinated axons was performed using Fiji from electron micrographs (cortical layer VI: 24–25 images per mouse; cortical layer I: 23–37 images per mouse; striatal WM: 10 images per mouse). The axon membrane was traced with the “Wand” tool or manually with the “Freehand selections” tool. The area of the shape was measured and the diameter was calculated using the formula: $d = 2\sqrt{a/\pi}$ (Figure 6B). Only axons transected in cross-section (as determined by the presence of neurofilament in the shape of dots rather than rods) were measured.

Statistical analysis—Statistical analysis and graphing were performed with Prism 7 software (GraphPad). Statistical comparisons in Figures 1–3 and 5 were performed using an unpaired two-tailed Student’s t test and in Figure 6 using a two-tailed Mann-Whitney test. Significance was determined by * $P < 0.05$. Data distribution was assumed to be normal, except in Figure 6, where a non-parametric test was used to account for the distribution of myelinated mEYFP+ axons. N values represent the number of mice in all figures except in Figure 6, where N represents the number of axons. Data are reported as mean ± s.e.m. when a Student’s t test was performed on the data; descriptive data are reported as mean ± s.d. Samples sizes and statistical details for each experiment are described in the figure legends.

Supplementary Material

Refer to Web version on PubMed Central for supplementary material.

ACKNOWLEDGMENTS

We thank Drs. Li Zhang (USC), Michael Bruchas (U Washington), and Jennifer Whistler (UC Davis) for providing mice. We thank Drs. Li He and Jennifer Whistler (UC Davis) for help in setting up the forced swim stress paradigm. We thank the Chan laboratory for their comments on the manuscript. We thank Ivy Hsieh (Cell Imaging Lab, San Francisco Veterans Affairs Medical Center) for her assistance with electron microscopy. We thank Dr. Sonia Mayoral for her support with revisions. This work was supported by funding from the NIH/NINDS (grants R01NS097428, and R01NS095889, and R01NS115746), the Adelson Medical Research Foundation (APND grant A130141), and the Rachleff family endowment to J.R.C. and the NSERC Doctoral Postgraduate Scholarship (PGSD3-487560-2016) and the Laura Gold Discovery Fellowship to L.A.O.

REFERENCES

Bacmeister CM, Barr HJ, McClain CR, Thornton MA, Nettles D, Welle CG, and Hughes EG (2020). Motor learning promotes remyelination via new and surviving oligodendrocytes. Nat. Neurosci 23, 819–831. [PubMed: 32424285]

Barak B, Zhang Z, Liu Y, Nir A, Trangle SS, Ennis M, Levandowski KM, Wang D, Quast K, Boulting GL, et al. (2019). Neuronal deletion of Gtf2i, associated with Williams syndrome, causes behavioral and myelin alterations rescuable by a remyelinating drug. Nat. Neurosci 22, 700–708. [PubMed: 31011227]

Bekinschtein P, Cammarota M, and Medina JH (2014). BDNF and memory processing. Neuropharmacology 76, 677–683. [PubMed: 23688925]

Bergles DE, and Richardson WD (2016). Oligodendrocyte Development and Plasticity. Cold Spring Harb. Perspect. Biol 8, a020453.

Bergles DE, Roberts DJ, Somogyi P, and Jahr CE (2000). Glutamatergic synapses on oligodendrocyte precursor cells in the hippocampus. Nature 405, 187–191. [PubMed: 10821275]

Bruchas MR, Xu M, and Chavkin C (2008). Repeated swim stress induces kappa opioid-mediated activation of extracellular signal-regulated kinase 1/2. Neuroreport 19, 1417–1422. [PubMed: 18766023]

Call CL, and Bergles DE (2021). Cortical neurons exhibit diverse myelination patterns that scale between mouse brain regions and regenerate after demyelination. Nat. Commun 12, 4767. [PubMed: 34362912]

Cheadle L, Rivera SA, Phelps JS, Ennis KA, Stevens B, Burkly LC, Lee W-CA, and Greenberg ME (2020). Sensory Experience Engages Microglia to Shape Neural Connectivity through a Non-Phagocytic Mechanism. Neuron 108, 451–468. [PubMed: 32931754]

Chefer VI, Bäckman CM, Gigante ED, and Shippenberg TS (2013). Kappa Opioid Receptors on Dopaminergic Neurons Are Necessary for Kappa-Mediated Place Aversion. Neuropsychopharmacology 38, 2623–2631. [PubMed: 23921954]

Cullen CL, Pepper RE, Clutterbuck MT, Pitman KA, Oorschot V, Auderset L, Tang AD, Ramm G, Emery B, Rodger J, et al. (2021). Periaxonal and nodal plasticities modulate action potential conduction in the adult mouse brain. Cell Rep. 34, 108641. [PubMed: 33472075]

Czopka T, Ffrench-Constant C, and Lyons DA (2013). Individual oligodendrocytes have only a few hours in which to generate new myelin sheaths in vivo. Dev. Cell 25, 599–609. [PubMed: 23806617]

Drake C, Terman G, Simmons M, Milner T, Kunkel D, Schwartzkroin P, and Chavkin C (1994). Dynorphin opioids present in dentate granule cells may function as retrograde inhibitory neurotransmitters. J. Neurosci 14, 3736–3750. [PubMed: 7911518]

Du C, Duan Y, Wei W, Cai Y, Chai H, Lv J, Du X, Zhu J, and Xie X (2016). Kappa opioid receptor activation alleviates experimental autoimmune encephalomyelitis and promotes oligodendrocyte-mediated remyelination. Nat. Commun 7, 11120. [PubMed: 27040771]

Duncan GJ, Manesh SB, Hilton BJ, Assinck P, Liu J, Moulson A, Plemel JR, and Tetzlaff W (2018). Locomotor recovery following contusive spinal cord injury does not require oligodendrocyte remyelination. Nat. Commun 9, 3066. [PubMed: 30076300]

Etxeberria A, Hokanson KC, Dao DQ, Mayoral SR, Mei F, Redmond SA, Ullian EM, and Chan JR (2016). Dynamic Modulation of Myelination in Response to Visual Stimuli Alters Optic Nerve Conduction Velocity. J. Neurosci 36, 6937–6948. [PubMed: 27358452]

Fu M, and Zuo Y (2011). Experience-dependent structural plasticity in the cortex. Trends Neurosci. 34, 177–187. [PubMed: 21397343]

Geraghty AC, Gibson EM, Ghanem RA, Greene JJ, Ocampo A, Goldstein AK, Ni L, Yang T, Marton RM, Paşca SP, et al. (2019). Loss of Adaptive Myelination Contributes to Methotrexate Chemotherapy-Related Cognitive Impairment. Neuron 103, 250–265. [PubMed: 31122677]

Gerfen C, Engber T, Mahan L, Susel Z, Chase T, Monsma F, and Sibley D (1990). D1 and D2 dopamine receptor-regulated gene expression of striatonigral and striatopallidal neurons. Science 250, 1429–1432. [PubMed: 2147780]

Gibson EM, Purger D, Mount CW, Goldstein AK, Lin GL, Wood LS, Inema I, Miller SE, Bieri G, Zuchero BJ, et al. (2014). Neuronal Activity Promotes Oligodendrogenesis and Adaptive Myelination in the Mammalian Brain. Science 344, 1252304. [PubMed: 24727982]

Goebbels S, Oltrogge JH, Kemper R, Heilmann I, Bormuth I, Wolfer S, Wichert SP, Möbius W, Liu X, Lappe-Siefke C, et al. (2010). Elevated phosphatidylinositol 3,4,5-trisphosphate in glia triggers cell-autonomous membrane wrapping and myelination. J. Neurosci 30, 8953–8964. [PubMed: 20592216]

Hill RA, Li AM, and Grutzendler J (2018). Lifelong cortical myelin plasticity and age-related degeneration in the live mammalian brain. Nat. Neurosci 21, 683–695. [PubMed: 29556031]

Hines JH, Ravanelli AM, Schwindt R, Scott EK, and Appel B (2015). Neuronal activity biases axon selection for myelination in vivo. Nat Neurosci 18, 683–689. [PubMed: 25849987]

Hippenmeyer S, Vrieseling E, Sigrist M, Portmann T, Laengle C, Ladle DR, and Arber S (2005). A Developmental Switch in the Response of DRG Neurons to ETS Transcription Factor Signaling. PLoS Biol. 3, e159. [PubMed: 15836427]

Horan P, Taylor J, Yamamura HI, and Porreca F (1992). Extremely long-lasting antagonistic actions of nor-binaltorphimine (nor-BNI) in the mouse tail-flick test. J. Pharmacol. Exp. Ther 260, 1237–1243. [PubMed: 1312164]

Hughes EG, Orthmann-Murphy JL, Langseth AJ, and Bergles DE (2018). Myelin remodeling through experience-dependent oligodendrogenesis in the adult somatosensory cortex. Nat. Neurosci 21, 696–706. [PubMed: 29556025]

Ibrahim LA, Huang JJ, Wang S-ZZ, Kim YJ, Zhang LI, and Tao HW (2018). Sparse Labeling and Neural Tracing in Brain Circuits by STARS Strategy: Revealing Morphological Development of Type II Spiral Ganglion Neurons. Cereb. Cortex 31, 2759–2772.

Jeffries MA, Urbanek K, Torres L, Wendell SG, Rubio ME, and Fyffe-Maricich SL (2016). ERK1/2 Activation in Preexisting Oligodendrocytes of Adult Mice Drives New Myelin Synthesis and Enhanced CNS Function. J. Neurosci 36, 9186–9200. [PubMed: 27581459]

Knoll AT, and Carlezon WA (2010). Dynorphin, stress, and depression. Brain Res. 1314, 56–73. [PubMed: 19782055]

Koudelka S, Voas MG, Almeida RG, Baraban M, Soetaert J, Meyer MP, Talbot WS, and Lyons DA (2016). Individual Neuronal Subtypes Exhibit Diversity in CNS Myelination Mediated by Synaptic Vesicle Release. Curr. Biol 26, 1447–1455. [PubMed: 27161502]

Krashes MJ, Shah BP, Madara JC, Olson DP, Strochlic DE, Garfield AS, Vong L, Pei H, Watabe-Uchida M, Uchida N, et al. (2014). An excitatory paraventricular nucleus to AgRP neuron circuit that drives hunger. Nature 507, 238–242. [PubMed: 24487620]

Lacoste B, Comin CH, Ben-Zvi A, Kaeser PS, Xu X, Costa L da F, and Gu C (2014). Sensory-Related Neural Activity Regulates the Structure of Vascular Networks in the Cerebral Cortex. Neuron 83, 1117–1130. [PubMed: 25155955]

Lee S, Leach MK, Redmond SA, Chong SY, Mellon SH, Tuck SJ, Feng Z-QQ, Corey JM, and Chan JR (2012). A culture system to study oligodendrocyte myelination processes using engineered nanofibers. Nat. Methods 9, 917–922. [PubMed: 22796663]

Lin S, and Bergles DE (2003). Synaptic signaling between GABAergic interneurons and oligodendrocyte precursor cells in the hippocampus. Nat. Neurosci 7, 24–32. [PubMed: 14661022]

Liu J, Dietz K, DeLoyht JM, Pedre X, Kelkar D, Kaur J, Vialou V, Lobo M, Dietz DM, Nestler EJ, et al. (2012). Impaired adult myelination in the prefrontal cortex of socially isolated mice. Nat. Neurosci 15, 1621–1623. [PubMed: 23143512]

Makinodan M, Rosen KM, Ito S, and Corfas G (2012). A Critical Period for Social Experience–Dependent Oligodendrocyte Maturation and Myelination. Science 337, 1357–1360. [PubMed: 22984073]

Martinez VK, Saldana-Morales F, Sun JJ, Zhu PJ, Costa-Mattioli M, and Ray RS (2019). Off-Target Effects of Clozapine-N-Oxide on the Chemosensory Reflex Are Masked by High Stress Levels. Front. Physiol 10, 521. [PubMed: 31178741]

McKenzie IA, Ohayon D, Li H, Faria J.P. de, Emery B, Tohyama K, and Richardson WD (2014). Motor skill learning requires active central myelination. Science 346, 318–322. [PubMed: 25324381]

McLaughlin J, Marton-Popovici M, and Chavkin C (2003). κ opioid receptor antagonism and prodynorphin gene disruption block stress-induced behavioral responses. J. Neurosci 23, 5674–5683. [PubMed: 12843270]

Mei F, Mayoral SR, Nobuta H, Wang F, Desponts C, Lorrain DS, Xiao L, Green AJ, Rowitch D, Whistler J, et al. (2016). Identification of the Kappa-Opioid Receptor as a Therapeutic Target for Oligodendrocyte Remyelination. J. Neurosci 36, 7925–7935. [PubMed: 27466337]

Mensch S, Baraban M, Almeida R, Czopka T, Ausborn J, Manira AE, and Lyons DA (2015). Synaptic vesicle release regulates myelin sheath number of individual oligodendrocytes in vivo. Nature Neuroscience 18, 628–630. [PubMed: 25849985]

Micheva KD, Wolman D, Mensh BD, Pax E, Buchanan J, Smith SJ, and Bock DD (2016). A large fraction of neocortical myelin ensheathes axons of local inhibitory neurons. eLife 5, e15784 [PubMed: 27383052]

Mitew S, Gobius I, Fenlon LR, McDougall SJ, Hawkes D, Xing YL, Bujalka H, Gundlach AL, Richards LJ, Kilpatrick TJ, et al. (2018). Pharmacogenetic stimulation of neuronal activity increases myelination in an axon-specific manner. Nat. Commun 9, 306. [PubMed: 29358753]

Murphy-Royal C, Johnston AD, Boyce AKJ, Diaz-Castro B, Institoris A, Peringod G, Zhang O, Stout RF, Spray DC, Thompson RJ, et al. (2020). Stress gates an astrocytic energy reservoir to impair synaptic plasticity. Nat. Commun 11, 2014. [PubMed: 32332733]

Muzumdar MD, Tasic B, Miyamichi K, Li L, and Luo L (2007). A global double-fluorescent Cre reporter mouse. Genesis 45, 593–605. [PubMed: 17868096]

Osso LA, and Chan JR (2017). Architecting the myelin landscape. Curr. Opin. Neurobiol 47, 1–7. [PubMed: 28709021]

Pan S, Mayoral SR, Choi HS, Chan JR, and Kheirbek MA (2020). Preservation of a remote fear memory requires new myelin formation. Nat. Neurosci 23, 487–499. [PubMed: 32042175]

Portoghese PS, Lipkowski AW, and Takemori AE (1987). Binaltorphimine and nor-binaltorphimine, potent and selective k-opioid receptor antagonists. Life Sci. 40, 1287–1292. [PubMed: 2882399]

Prigge JR, Wiley JA, Talago EA, Young EM, Johns LL, Kundert JA, Sonsteng KM, Halford WP, Capecchi MR, and Schmidt EE (2013). Nuclear double-fluorescent reporter for in vivo and ex vivo analyses of biological transitions in mouse nuclei. Mamm. Genome 24, 389–399.

Schindler AG, Messinger DI, Smith JS, Shankar H, Gustin RM, Schattauer SS, Lemos JC, Chavkin NW, Hagan CE, Neumaier JF, et al. (2012). Stress produces aversion and potentiates cocaine reward by releasing endogenous dynorphins in the ventral striatum to locally stimulate serotonin reuptake. J. Neurosci 32, 17582–17596. [PubMed: 23223282]

Schüller U, Heine VM, Mao J, Kho AT, Dillon AK, Han Y-G, Huillard E, Sun T, Ligon AH, Qian Y, et al. (2008). Acquisition of Granule Neuron Precursor Identity Is a Critical Determinant of Progenitor Cell Competence to Form Shh-Induced Medulloblastoma. Cancer Cell 14, 123–134. [PubMed: 18691547]

Schwarzer C (2009). 30 years of dynorphins--new insights on their functions in neuropsychiatric diseases. Pharmacol. Ther 123, 353–370. [PubMed: 19481570]

Sharifi N, Diehl N, Yaswen L, Brennan MB, and Hochgeschwender U (2001). Generation of dynorphin knockout mice. Brain Research. Mol. Brain Res 86, 70–75. [PubMed: 11165373]

Simmons ML, Terman GW, Gibbs SM, and Chavkin C (1995). L-type calcium channels mediate dynorphin neuropeptide release from dendrites but not axons of hippocampal granule cells. Neuron 14, 1265–1272. [PubMed: 7605635]

Sohn J, Hioki H, Okamoto S, and Kaneko T (2014). Preprodynorphin-expressing neurons constitute a large subgroup of somatostatin-expressing GABAergic interneurons in the mouse neocortex. J. Comp. Neurol 522, 1506–1526. [PubMed: 24122731]

Steadman PE, Xia F, Ahmed M, Mocle AJ, Penning ARA, Geraghty AC, Steenland HW, Monje M, Josselyn SA, and Frankland PW (2020). Disruption of Oligodendrogenesis Impairs Memory Consolidation in Adult Mice. Neuron 105, 1–15. [PubMed: 31951525]

Stedehouder J, Brizee D, Slotman JA, Pascual-Garcia M, Leyrer ML, Bouwen BL, Dirven CM, Gao Z, Berson DM, Houtsmuller AB, et al. (2019). Local axonal morphology guides the topography of interneuron myelination in mouse and human neocortex. eLife 8, e48615. [PubMed: 31742557]

Sturrock RR (1980). Myelination of the mouse corpus callosum. Neuropathol. Appl. Neurobiol 6, 415–420. [PubMed: 7453945]

Swire M, Kotelevtsev Y, Webb DJ, Lyons DA, and Ffrench-Constant C (2019). Endothelin signalling mediates experience-dependent myelination in the CNS. eLife 8, e49493. [PubMed: 31657718]

Takeuchi T, Duszkiewicz AJ, and Morris RGM (2014). The synaptic plasticity and memory hypothesis: encoding, storage and persistence. Philos. Trans. R. Soc. Lond., B, Biol. Sci 369, 20130288. [PubMed: 24298167]

Terman G, Wagner J, and Chavkin C (1994). Kappa Opioids Inhibit Induction of Long-Term Potentiation in the Dentate Gyrus of the Guinea Pig Hippocampus. J. Neurosci 14, 4740–4747. [PubMed: 7913954]

Tomassy G, Berger DR, Chen H-H, Kasthuri N, Hayworth KJ, Vercelli A, Seung SH, Lichtman JW, and Arlotta P (2014). Distinct Profiles of Myelin Distribution Along Single Axons of Pyramidal Neurons in the Neocortex. Science 344, 319–324. [PubMed: 24744380]

Tremblay R, Lee S, and Rudy B (2016). GABAergic Interneurons in the Neocortex: From Cellular Properties to Circuits. Neuron 91, 260–292. [PubMed: 27477017]

Von Voigtlander PF, Lahti RA, and Ludens JH (1983). U-50,488: a selective and structurally novel non-Mu (kappa) opioid agonist. J. Pharmacol. Exp. Ther 224, 7–12. [PubMed: 6129321]

Wang F, Ren S-Y, Chen J-F, Liu K, Li R-X, Li Z-F, Hu B, Niu J-Q, Xiao L, Chan JR, et al. (2020). Myelin degeneration and diminished myelin renewal contribute to age-related deficits in memory. Nat. Neurosci 23, 481–486. [PubMed: 32042174]

Whiteus C, Freitas C, and Grutzendler J (2014). Perturbed neural activity disrupts cerebral angiogenesis during a postnatal critical period. Nature 505, 407–411. [PubMed: 24305053]

Xiao L, Ohayon D, McKenzie IA, Sinclair-Wilson A, Wright JL, Fudge AD, Emery B, Li H, and Richardson WD (2016). Rapid production of new oligodendrocytes is required in the earliest stages of motor-skill learning. Nat. Neurosci 19, 1210–1217. [PubMed: 27455109]

Xin W, and Chan JR (2020). Myelin plasticity: sculpting circuits in learning and memory. Nat. Rev. Neurosci 21, 682–694. [PubMed: 33046886]

Yakovleva T, Bazov I, Cebers G, Marinova Z, Hara Y, Ahmed A, Vlaskovska M, Johansson B, Hochgeschwender U, Singh IN, et al. (2006). Prodynorphin storage and processing in axon terminals and dendrites. FASEB J. 20, 2124–2126. [PubMed: 16966485]

Yang SM, Michel K, Jokhi V, Nedivi E, and Arlotta P (2020). Neuron class-specific responses govern adaptive myelin remodeling in the neocortex. Science 370, eabd2109. [PubMed: 33335032]

Young KM, Psachoulia K, Tripathi RB, Dunn S-JJ, Cossell L, Attwell D, Tohyama K, and Richardson WD (2013). Oligodendrocyte dynamics in the healthy adult CNS: evidence for myelin remodeling. Neuron 77, 873–885. [PubMed: 23473318]

Zhu X, Hill RA, Dietrich D, Komitova M, Suzuki R, and Nishiyama A (2011). Age-dependent fate and lineage restriction of single NG2 cells. Development 138, 745–753. [PubMed: 21266410]

HIGHLIGHTS

- Forced swim stress promotes experience-dependent OPC differentiation
- Stress-induced OPC differentiation is mediated by the neuropeptide dynorphin
- Dynorphin promotes developmental OPC differentiation
- The axons of dynorphin-expressing neurons are unmyelinated

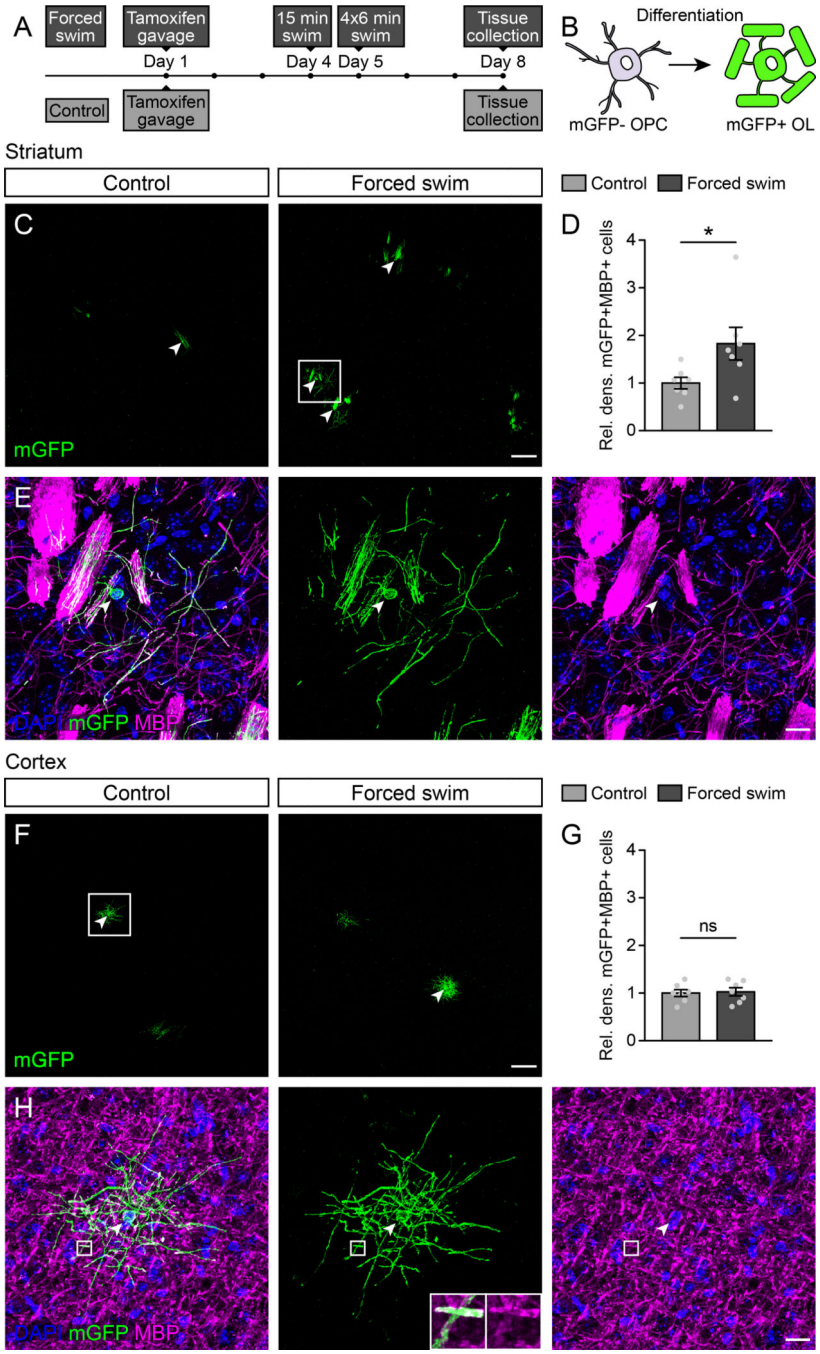

Figure 1. Forced swim stress promotes striatal OPC differentiation and myelination

(A) Experimental paradigm performed in 12–16 wk old *Cspg4*-CreER™; *Mapt*-mGFP littermates.

(B) Newly differentiated mGFP+ oligodendrocytes following tamoxifen administration. Abbreviation: OL = oligodendrocyte.

(C) Representative images of mGFP+ oligodendrocytes in control and forced swim stressed mice in striatum. Cell somas were quantified (arrowheads). Box enlarged in (E).

(D) Quantification of relative density of mGFP+MBP+ cells in striatum in control vs. forced swim stressed mice (both groups: n = 7; control: 1.000 ± 0.1202, forced swim: 1.827 ± 0.3423; P = 0.0418, t(12) = 2.279).
(E) Enlarged mGFP+ oligodendrocyte from (C) colocalizing with DAPI and MBP.
(F) Representative images in cortex. Box enlarged in (H).
(G) Quantification in cortex (both groups: n = 7; control: 1.000 ± 0.07325, forced swim: 1.026 ± 0.08559; P = 0.8240, t(12) = 0.2274).
(H) Enlargement from (F). Box around mGFP+MBP+ myelin segment enlarged in 7.5 μm insets.
Scale bars, (C) and (F), 100 μm; (E) and (H), 15 μm.
Data presented as mean ± s.e.m.; two-tailed Student's t test; *P < 0.05; ns = not significant.
See Figures S2 and S7.

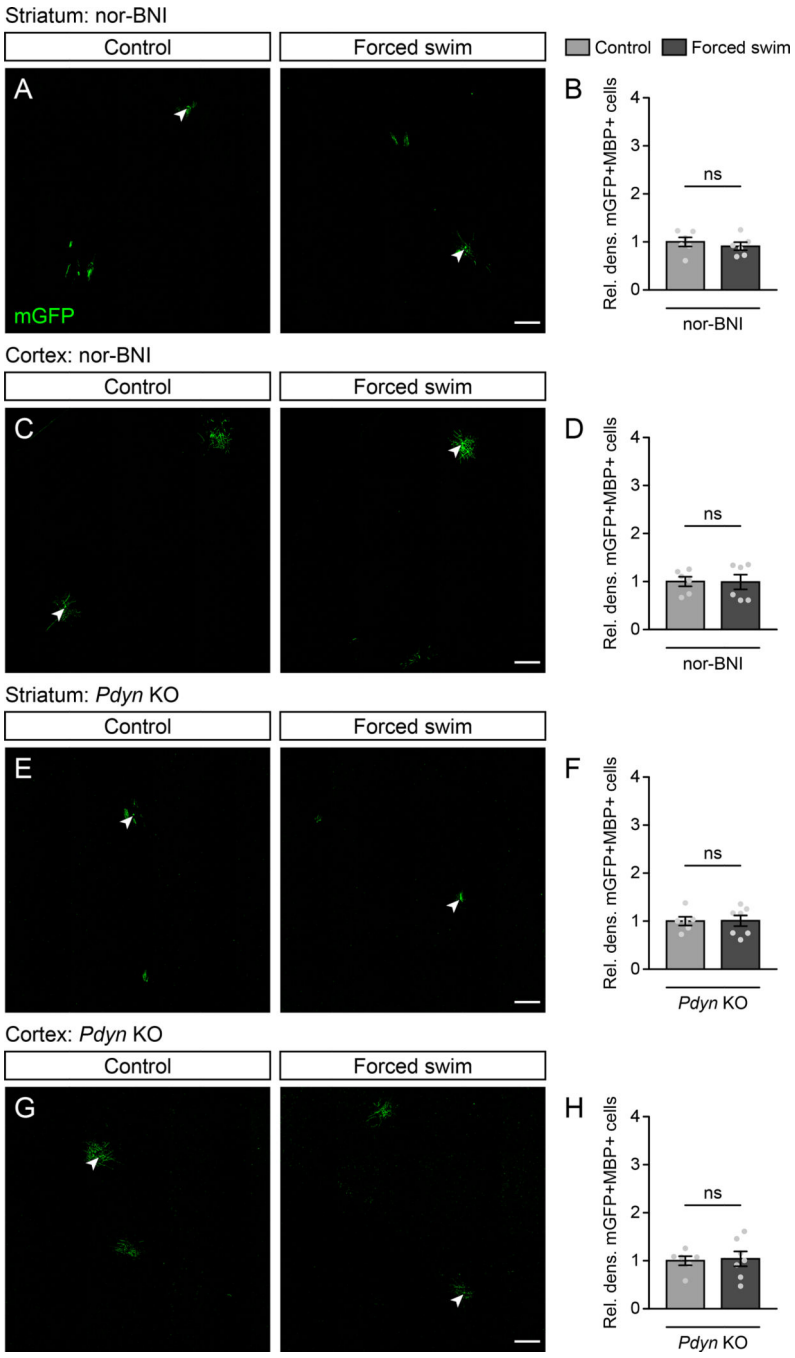

Figure 2. Blocking dynorphin-KOR signaling prevents stress-induced OPC differentiation and myelination

(A) Representative images of mGFP+ oligodendrocytes in striatum of control and forced swim stressed 12–16 wk old *Cspg4*-CreER™; *Mapt*-mGFP littermates given nor-BNI.

(B) Quantification of relative density of mGFP+MBP+ cells in striatum of mice described in (A) (both groups: n = 6; control: 1.000 ± 0.09525; forced swim: 0.911 ± 0.08374; P = 0.4989, t(10) = 0.7016).

(C) Representative images in cortex of mice described in (A).

(D) Quantification in cortex of mice described in (A) (both groups: n = 6; control: 1.000 ± 0.09924; forced swim: 0.9895 ± 0.1528; P = 0.9553, t(10) = 0.05751).
(E) Representative images of mGFP+ oligodendrocytes in striatum of control and forced swim stressed 12–16 wk old *Cspg4*-CreER™; *Mapt*-mGFP; *Pdyn* KO littermates.
(F) Quantification of relative density of mGFP+MBP+ cells in striatum of mice described in (E) (control: 1.000 ± 0.08924, n = 6; forced swim: 1.008 ± 0.1113, n = 7; P = 0.9579, t(11) = 0.05397).
(G) Representative images in cortex of mice described in (E).
(H) Quantification in cortex of mice described in (E) (control: 1.000 ± 0.0939, n = 6; forced swim: 1.04 ± 0.1546, n = 7; P = 0.8359, t(11) = 0.2121).
Scale bars, 100 μm.
Data presented as mean ± s.e.m.; two-tailed Student's t test; *P < 0.05; ns = not significant.

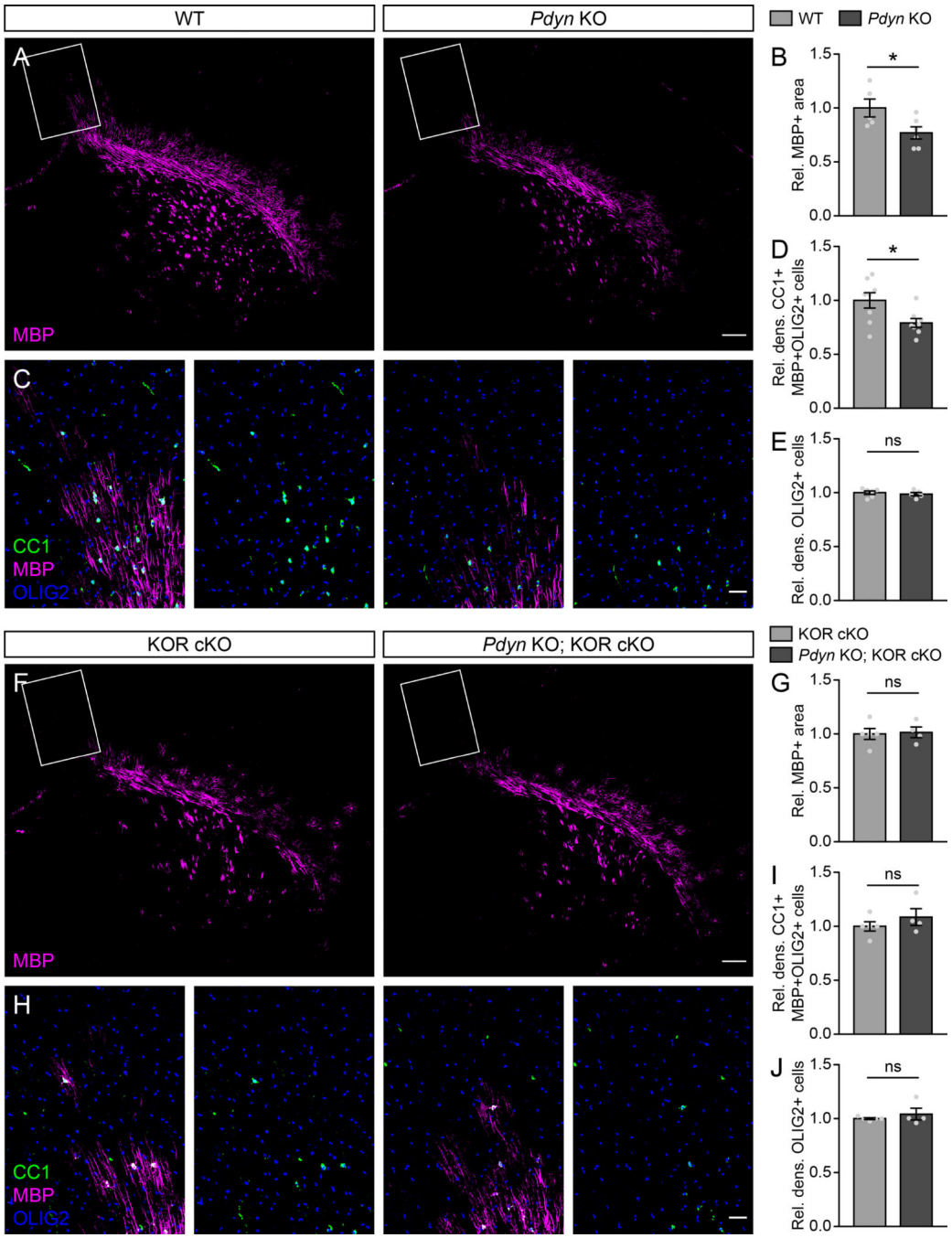

Figure 3. Dynorphin knock-out mice have deficits in developmental OPC differentiation and myelination redundant with the loss of OPC KORs

(A) Representative images of MBP immunostaining in MBP quantification region in P8 wild-type (WT) and *Pdyn* KO littermates. Box indicates quantification region for CC1+OLIG2+ and OLIG2+ cells in (C).

(B) Quantification of relative MBP area (WT: 1.000 ± 0.08261, n = 5; *Pdyn* KO: 0.7693 ± 0.05614, n = 6; P = 0.0414, t(9) = 2.378).

(C) Representative images of MBP, CC1, and OLIG2 immunostaining in the quantification region for CC1+MBP+OLIG2+ and OLIG2+ cells in P8 WT and *Pdyn* KO littermates.
(D-E) Quantification of relative density of CC1+MBP+OLIG2+ cells (both groups: n = 8; WT: 1.0000 ± 0.07106; *Pdyn* KO: 0.7914 ± 0.04061; P = 0.0232, t(14) = 2.548) (D) and OLIG2+ cells (WT: 1.0000 ± 0.01643, n = 6; *Pdyn* KO: 0.9866 ± 0.01563, n = 5; P = 0.5754, t(9) = 0.5812) (E).
(F) Representative images of MBP immunostaining as described in (A) in P8 KOR cKO and *Pdyn* KO; KOR cKO littermates.
(G) Quantification of relative MBP area (KOR cKO: 1.0000 ± 0.05024, n = 5; *Pdyn* KO; KOR cKO: 1.015 ± 0.0493, n = 4; P = 0.8445, t(7) = 0.2036).
(H) Representative images of MBP, CC1, and OLIG2 immunostaining as described in (C) in P8 KOR cKO and *Pdyn* KO; KOR cKO littermates.
(I-J) Quantification of relative density of CC1+MBP+OLIG2+ cells (KOR cKO: 1.0000 ± 0.04294, n = 5; *Pdyn* KO; KOR cKO: 1.086 ± 0.07834, n = 4; P = 0.3406, t(7) = 1.022) (I) and OLIG2+ cells (KOR cKO: 1.0000 ± 0.007635, n = 5; KOR cKO; *Pdyn* KO: 1.042 ± 0.05419, n = 4; P = 0.4119, t(7) = 0.8724) (J).
Scale bars, (A) and (F), 200 μm; (C) and (H) 50 μm.
Data presented as mean ± s.e.m.; two-tailed Student's t test; *P < 0.05; ns = not significant.
See Figure S1.

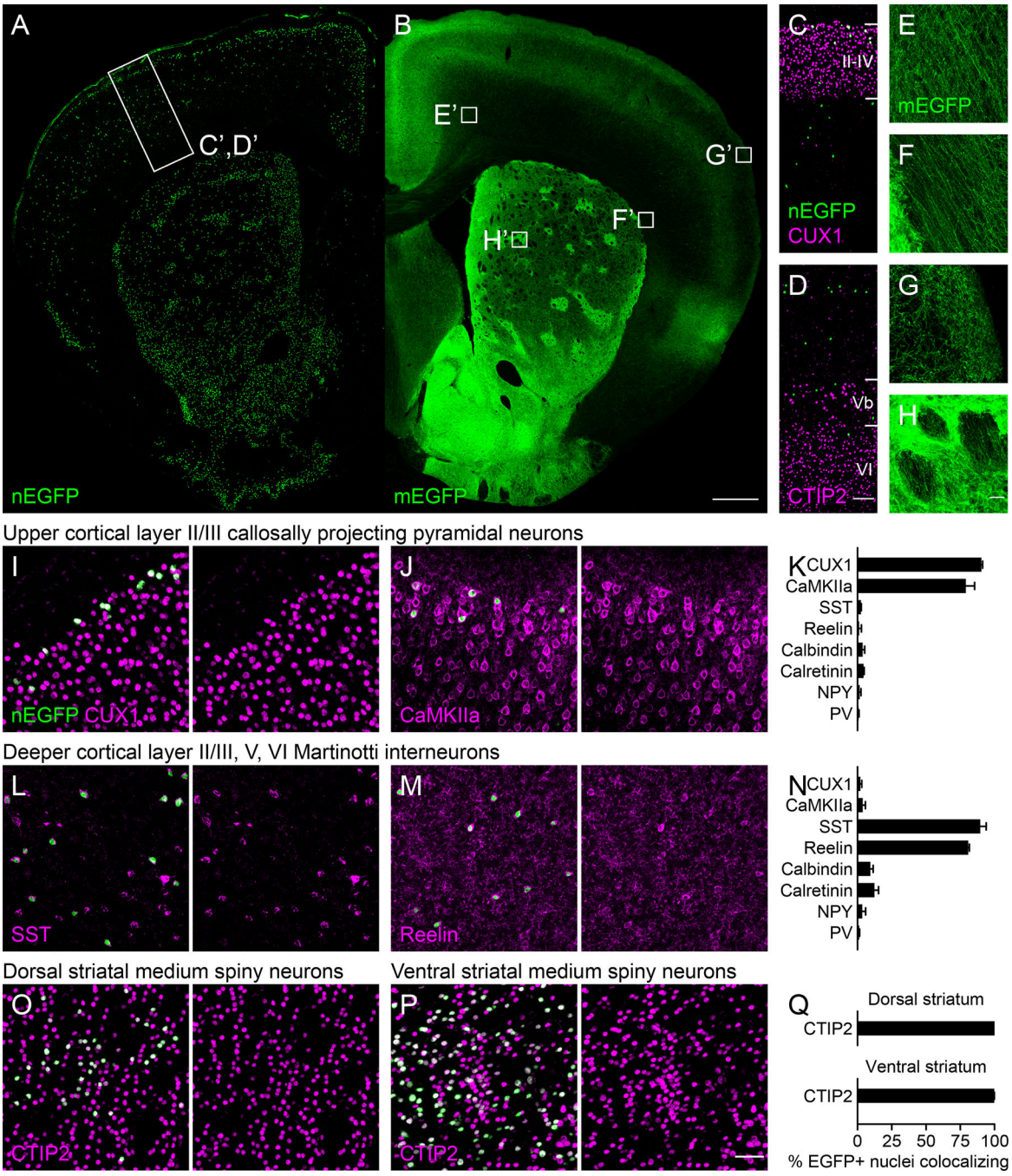

Figure 4. Identification of several neuronal subtypes expressing dynorphin

(A-B) Representative images of nEGFP (A) and mEGFP (B) immunostaining in coronal sections of 12–16 wk old *Pdyn*-Cre; nTnG (A) or *Pdyn*-Cre; mTmG (B) mice. Boxes enlarged in (C-H).

(C-D) Representative images showing two populations of nEGFP+ cells, localized by layer markers CUX1 (C) and CTIP2 (D).

(E-H) Representative images of mEGFP+ axon tracts.

(I-J) Representative images of colocalization of upper layer II/III nEGFP+ cells with CUX1 (I) and CaMKIIa (J).

(K) Percentage of upper cortical layer II/III nEGFP+ cells colocalizing with neuronal markers in n = 2 mice.

(L-M) Representative images of colocalization of deeper cortical layer nEGFP+ cells with somatostatin (SST) (L) and reelin (M).

(N) Percentage of deeper cortical layer nEGFP+ cells colocalizing with neuronal markers in n = 2 mice.

(O-P) Representative images of colocalization of dorsal (O) and ventral (P) striatal nEGFP+ cells with CTIP2.

(Q) Percentage of striatal nEGFP+ cells colocalizing with CTIP2 in n = 2 mice.

Abbreviations: NPY = neuropeptide Y; PV = parvalbumin.

Scale bars, (A) and (B), 500 μm; (C) and (D), 100 μm; (E-H), 20 μm; (I-J) and (L-M) and (O-P), 50 μm.

Data presented as mean ± s.d.

See Figures S2–S5.

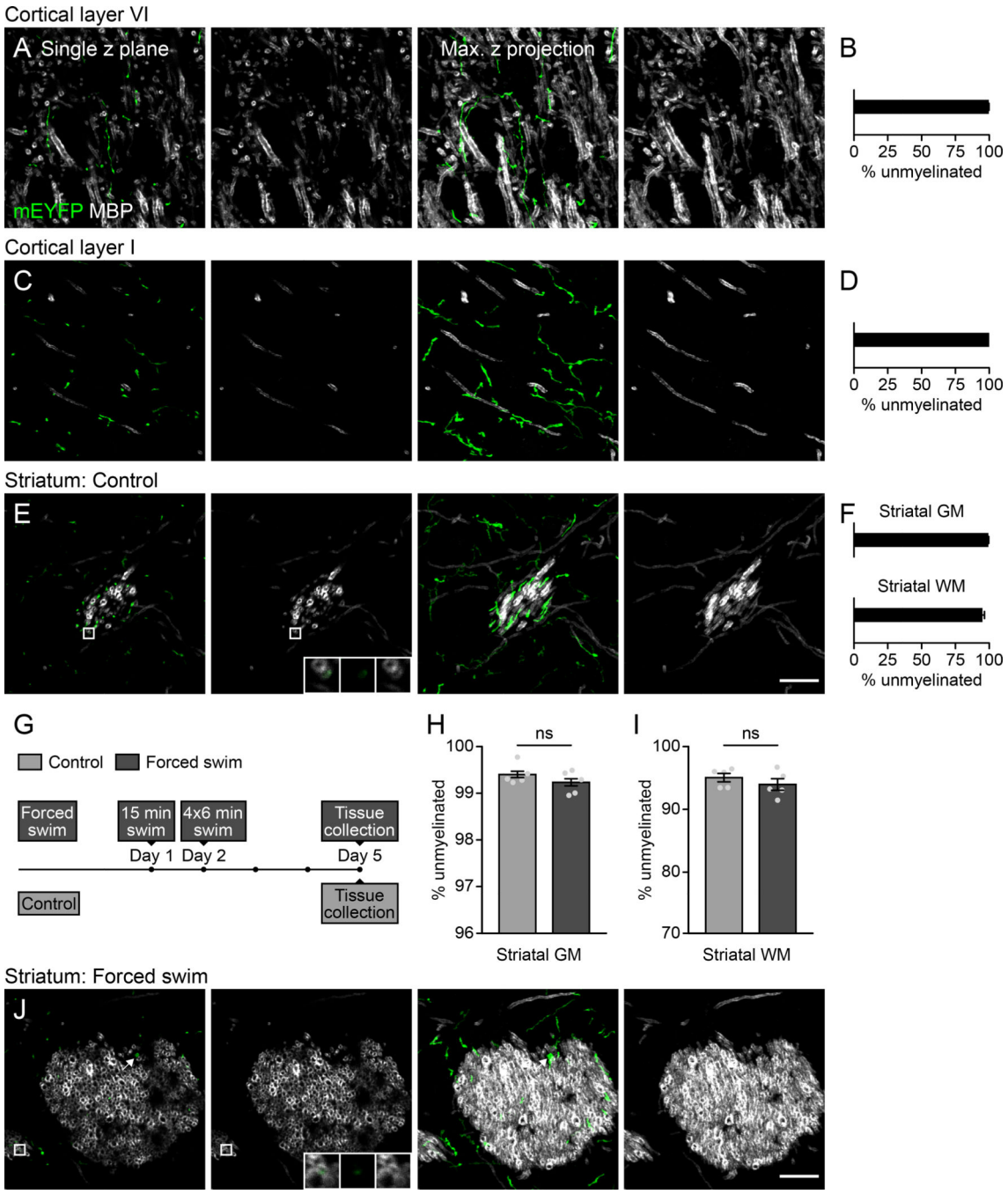

Figure 5. Axons of dynorphin-expressing neurons are unmyelinated normally and following forced swim stress

(A) Representative images of immunostaining for mEYFP and MBP in cortical layer VI in 12–16 wk old *Pdyn*-Cre; STARS mice. Left: single z plane; right: 6 μm depth maximum intensity z projections.

(B) Quantification of percentage of unmyelinated mEYFP+ axons in cortical layer VI (3950/3960 axons, n = 3 mice).

(C) Representative images of cortical layer I.

(D) Quantification in cortical layer I (5549/5549 axons, n = 3 mice).
(E) Representative images of striatum. Box around myelinated mEYFP+ axon enlarged in 2.6 μm insets.
(F) Quantification in striatal gray matter (8902/8967 axons, n = 5 mice) and white matter (1457/1543 axons, n = 5 mice).
(G) Experimental paradigm for forced swim stress and tissue collection performed in 12–16 wk old *Pdyn*-Cre; STARS littermates.
(H-I) Quantification of percentage of unmyelinated mEYFP+ axons in control vs. forced swim stressed littermates in striatal gray matter (both groups: n = 5, control: 99.4 ± 0.09768; forced swim: 99.24 ± 0.1094; P = 0.2863, t(8) = 1.143) (H) and white matter (both groups: n = 5, control: 95.01 ± 0.6661; forced swim: 93.91 ± 0.9236; P = 0.3601, t(8) = 0.9707) (I).
(J) Representative images of immunostaining for mEYFP and MBP in striatum of 12–16 wk old forced swim stressed *Pdyn*-Cre; STARS mice. Box around myelinated mEYFP+ axon enlarged in 2.6 μm insets. mEYFP+ dendrites (arrow) were excluded from quantification. Scale bars, 10 μm.
Data in (B), (D), and (F) presented as mean ± s.d.; data in (H-I) presented as mean ± s.e.m.; two-tailed Student's t test; *P < 0.05; ns = not significant.
See Figure S6.

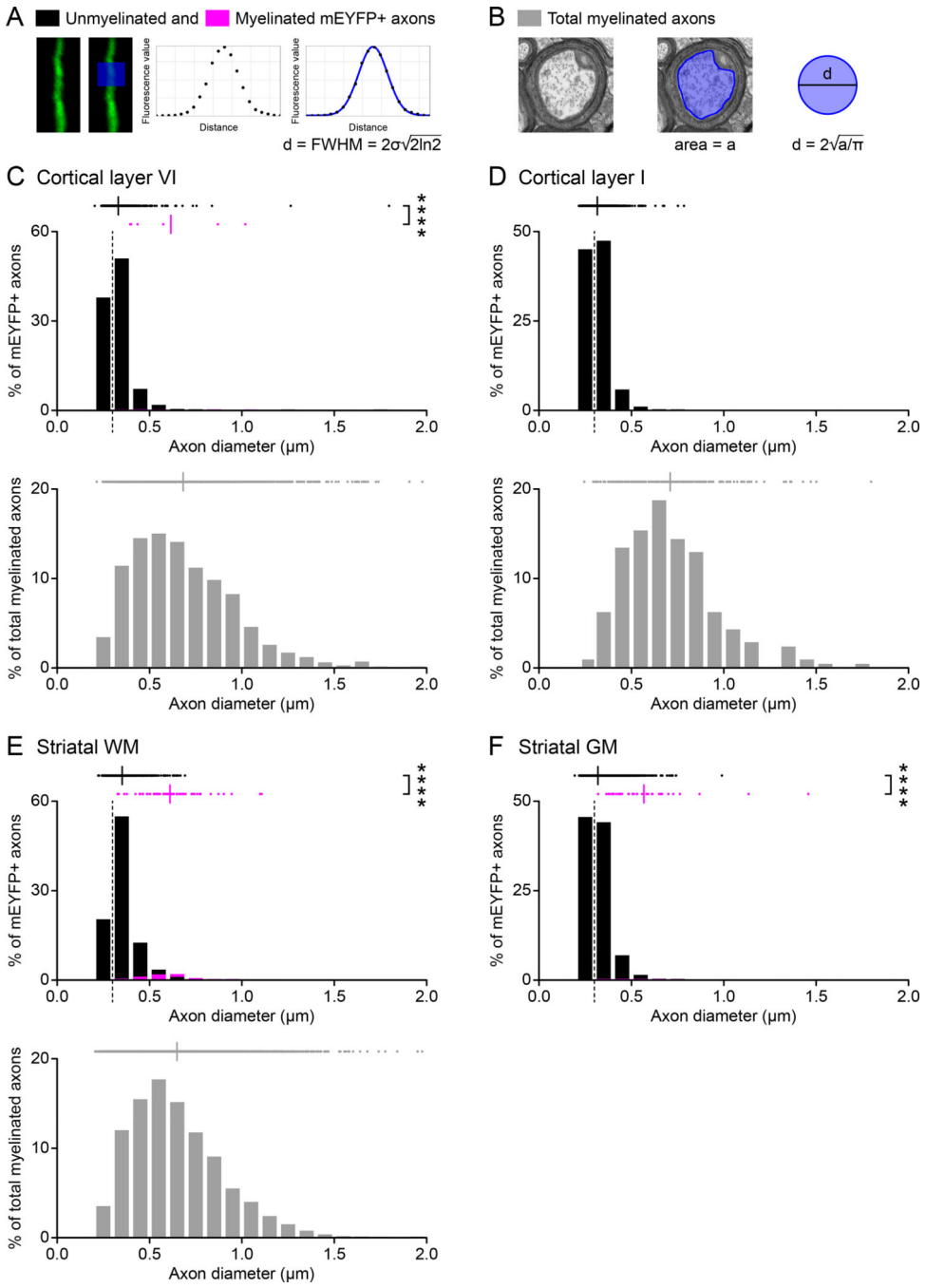

Figure 6. The axons of unmyelinated dynorphin-expressing neurons are of smaller diameter than myelinated axons

(A) Method for measuring diameters of mEYFP+ unmyelinated and myelinated axons. Image width, 1.75 µm. Blue box height, 1 µm.

(B) Method for measuring diameters of myelinated axons from electron micrographs. Image width, 1.6 µm.

(C) Top: Aligned dot plot (with mean) of axon diameters of unmyelinated (black) and myelinated (magenta) mEYFP+ axons in cortical layer VI (unmyelinated: median = 0.3128,

n = 817 axons; myelinated: median = 0.5056, n = 6 axons; U = 240, P < 0.0001) from n = 3 mice. Histogram of the same data binned into 0.1 μm bins. Dotted line at 0.3 μm indicates the oligodendrocyte myelination threshold. Bottom: Aligned dot plot (with mean) and histogram with 0.1 μm bins of diameters of myelinated axons from electron micrographs (gray) in cortical layer VI (n = 1390 axons) from n = 4 mice.

(D) Top: Aligned dot plot (with mean) of axon diameters of unmyelinated mEYFP+ axons (n = 1259 axons) and histogram of cortical layer I in n = 3 mice. Bottom: Aligned dot plot (with mean) and histogram of diameters of myelinated axons from electron micrographs in cortical layer I (n = 208 axons) from n = 4 mice.

(E) Top: Aligned dot plot (with mean) of mEYFP+ axon diameters (unmyelinated: median = 0.3402, n = 756 axons; myelinated: median = 0.5987, n = 59 axons; U = 2342, P < 0.0001) and histogram of striatal WM from n = 5 mice. Bottom: Aligned dot plot (with mean) and histogram of diameters of myelinated axons from electron micrographs in striatal WM (n = 3597 axons) from n = 3 mice.

(F) Aligned dot plot (with mean) of mEYFP+ axon diameters (unmyelinated: median = 0.3051, n = 3259 axons; myelinated: median = 0.5123, n = 36 axons; U = 5466, P < 0.0001) and histogram of striatal GM from n = 5 mice.

Two-tailed Mann-Whitney test; **** P < 0.0001.

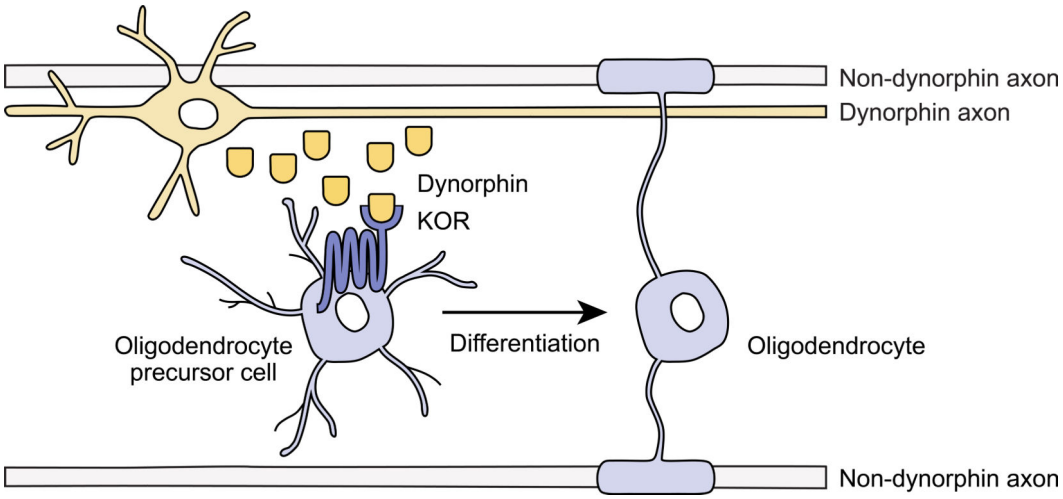

Figure 7. Model of dynorphin-induced OPC differentiation and subsequent myelination of axons of non-dynorphin expressing neurons

During development and forced swim stress, small axonal diameter dynorphin-expressing neurons release dynorphin. Dynorphin binds KORs on OPCs causing OPCs to differentiate into myelinating oligodendrocytes, which myelinate the axons of non-dynorphin-expressing neurons.

KEY RESOURCES TABLE

REAGENT or RESOURCE	SOURCE	IDENTIFIER
Antibodies		
Rat monoclocal anti-myelin basic protein (MBP), 1:600	EMD Millipore	Cat # MAB386, RRID:AB_94975
Rabbit monoclonal anti-GFP, 1:500	Thermo Fisher Scientific	Cat # G10362, RRID:AB_2536526
Chicken polyclonal anti-GFP, 1:1000	Rockland Immunochemicals	Cat # 600-901-215, RRID:AB_1537402
Rabbit polyclonal anti-OLIG2, 1:1000	EMD Millipore	Cat # AB9610, RRID:AB_570666
Mouse monoclonal CC1, 1:500	EMD Millipore	Cat # OP80, RRID:AB_2057371
Rabbit polyclonal anti-CUX1, 1:200	Santa Cruz Biotechnology	Cat # sc-13024, RRID:AB_2261231
Rat monoclonal anti-CTIP2, 1:500	Abcam	Cat # ab18465, RRID:AB_2064130
Mouse monoclonal anti-CaMKIIa, 1:50	Santa Cruz Biotechnology	Cat # sc-13141, RRID:AB_626789
Rabbit polyclonal anti-somatostatin (SST), 1:500	Santa Cruz Biotechnology	Cat # T-4103, RRID:AB_518614
Mouse monoclonal anti-reelin, 1:1000	EMD Millipore	Cat # MAB5364, RRID:AB_2179313
Mouse monoclonal anti-calbindin, 1:500	Swant	Cat # 300, RRID: AB_10000347
Mouse monoclonal anti-calretinin, 1:500	EMD Millipore	Cat # MAB1568, RRID:AB_94259
Rabbit monoclonal anti-neuropeptide Y (NPY), 1:1000	Cell Signaling Technology	Cat # 11976, RRID:AB_2716286
Rabbit polyclonal anti-parvalbumin (PV), 1:500	Swant	Cat # PV 27, RRID:AB_2631173
Rat monoclonal anti-CD140a/ PDGFRα, 1:500	BD Biosciences	Cat # 558774, RRID:AB_397117
Rabbit polyclonal anti-aspartoacylase (ASPA), 1:500	EMD Millipore	Cat # ABN1698, RRID:AB_2827931
Rabbit polyclonal anti-aspartoacylase (ASPA), 1:1000	GeneTex	Cat # GTX113389, RRID:AB_2036283
Goat polyclonal anti-SOX9, 1:100	R&D Systems	Cat # AF3075, RRID:AB_2194160
Rabbit polyclonal anti-IBA1, 1:1000	Wako	Cat # 019–19741, RRID:AB_839504
Goat anti-rabbit AlexaFluor 488, 1:1000	Thermo Fisher Scientific	Cat # A-11034, RRID:AB_2576217
Donkey anti-rabbit AlexaFluor 488, 1:1000	Thermo Fisher Scientific	Cat # A-21206, RRID:AB_2535792
Goat anti-rabbit AlexaFluor 647, 1:1000	Thermo Fisher Scientific	Cat # A-21245, RRID:AB_2535813
Goat anti-rat AlexaFluor 594, 1:1000	Thermo Fisher Scientific	Cat # A-11007, RRID:AB_10561522
Goat anti-rat AlexaFluor 594, 1:800	Jackson ImmunoResearch	Cat # 112-585-167, RRID:AB_2338383
Goat anti-rat AlexaFluor 647, 1:1000	Thermo Fisher Scientific	Cat # A-21247, RRID:AB_141778
Goat anti-mouse AlexaFluor 488, 1:800	Jackson ImmunoResearch	Cat # 115-545-166, RRID:AB_2338852
Goat anti-mouse AlexaFluor 647, 1:1000	Thermo Fisher Scientific	Cat # A-21236, RRID:AB_2535805
Goat anti-chicken AlexaFluor 488, 1:1000	Thermo Fisher Scientific	Cat # A-11039, RRID:AB_142924
Donkey anti-goat AlexaFluor 647, 1:1000	Thermo Fisher Scientific	Cat # A-21447, RRID:AB_141844
Chemicals, Peptides, and Recombinant Proteins		
DAPI	Thermo Fisher Scientific	Cat # D1306
Normal goat serum (NGS)	Sigma-Aldrich	Cat # G9023
Normal donkey serum (NDS)	Sigma-Aldrich	Cat # D9663
Triton X-100	Sigma-Aldrich	Cat # T8787
L.A.B. Solution	Polysciences	Cat # 24310–500
Glycergel Mounting Medium	Agilent	Cat # C0563
Tamoxifen	Sigma-Aldrich	Cat # T5648

REAGENT or RESOURCE	SOURCE	IDENTIFIER
nor-Binaltorphimine dihydrochloride (nor-BNI)	Sigma-Aldrich	Cat # N1771
(±)-U-50488 hydrochloride	Tocris	Cat # 0495
2,2,2-tribromoethyl alcohol	Sigma-Aldrich	Cat # T48402
Paraformaldehyde (PFA)	Electron Microscopy Sciences	Cat # 19210
Sodium azide	BioExpress	Cat # 0639
Experimental Models: Organisms/Strains		
Mouse: *Cspg4*-CreER™: B6.Cg-Tg(Cspg4-cre/Esr1*)BAkik/J	Zhu et al., 2011	RRID:IMSR_JAX:008538
Mouse: *Mapt*-mGFP: B6;129P2-*Mapttm2Arbr*/J	Hippenmeyer et al., 2005	RRID:IMSR_JAX:021162
Mouse: *Pdyn* KO: B6.129S4-Pdyntm1Ute/J	Sharifi et al., 2001	RRID:IMSR_JAX:004272
Mouse: *Olig2*-Cre: STOCK *Olig2*$^{tm2(TVA,cre)Rth}$/J	Schüller et al., 2008	RRID:IMSR_JAX:011103
Mouse: *Oprk1*-loxP: B6-Kor tm2Jlw/NTac	Chefer et al., 2013	N/A
Mouse: *Pdyn*-Cre: B6;129S-Pdyntm1.1(cre)Mjkr/LowlJ	Krashes et al., 2014	RRID:IMSR_JAX:027958
Mouse: nTnG: B6N.129S6-Gt(ROSA)26Sortm1(CAG-tdTomato*,-EGFP*)Ees/J	Prigge et al., 2013	RRID:IMSR_JAX:023537
Mouse: mTmG: B6.129(Cg)-Gt(ROSA)26Sortm4(ACTB-tdTomato,-EGFP)Luo/J	Muzumdar et al. 2007	RRID:IMSR_JAX:007676
Mouse: STARS: STOCK Gt(ROSA)26Sortm1(CAG-mCherry,-EYFP*)Liiz/J	Ibrahim et al., 2018	RRID:IMSR_JAX:032453
Oligonucleotides		
See Table S1 for primers.		
Software and Algorithms		
Fiji	NIH	RRID:SCR_002285
Imaris 9.3.0	Bitplane	RRID:SCR_007370
GraphPad Prism 7	GraphPad	RRID:SCR_002798
Adobe Illustrator CC 2017	Adobe	RRID:SCR_010279
Other		
Zeiss Axio Scan Z1 Slide Scanner	Zeiss	N/A
Zeiss LSM 700 laser scanning confocal microscope	Zeiss	N/A
Zeiss Axio Imager M2 microscope	Zeiss	N/A